

Spatiotemporal Coverage in Fusion-based Sensor Networks

Rui Tan and Guoliang Xing

Abstract Wireless sensor networks (WSNs) have been increasingly available for critical applications such as security surveillance and environmental monitoring. As a fundamental performance measure of WSNs, *coverage* characterizes how well a sensing field is monitored by a network. Two facets of coverage, *i.e.*, *spatial coverage* and *temporal coverage*, quantify the percentage of area that is well monitored by the network and the timeliness of the network in detecting targets appearing in the sensing field, respectively. Although advanced collaborative signal processing algorithms have been adopted by many existing WSNs, most previous analytical studies on spatiotemporal coverage of WSNs are conducted based on overly simplistic sensing models (*e.g.*, the disc model) that do not capture the stochastic nature of sensing. In this chapter, we attempt to bridge this gap by exploring the fundamental limits of spatiotemporal coverage based on stochastic *data fusion* models that fuse *noisy* measurements of multiple sensors. We derive the scaling laws between spatiotemporal coverage, network density, and signal-to-noise ratio (SNR). We show that data fusion can significantly improve spatiotemporal coverage by exploiting the collaboration among sensors when several physical properties of the target signal are known. In particular, for signal path loss exponent of k (typically between 2.0 and 5.0), we prove that $\rho_f/\rho_d = \mathcal{O}(\delta^{2/k})$, where ρ_f and ρ_d are the densities of uniformly deployed sensors that achieve full spatial coverage or minimum detection delay under the fusion and disc models, respectively, and δ is SNR. Our results help understand the limitations of the previous analytical results based on the disc model and provide key insights into the design of WSNs that adopt data

Rui Tan

Advanced Digital Sciences Center, Singapore, e-mail: tanrui@adsc.com.sg
(Part of this book chapter was written when Rui Tan was with Michigan State University.)

Guoliang Xing

Michigan State University, East Lansing, MI 48824, USA, e-mail: glxing@msu.edu

The work presented in this chapter was supported in part by the National Science Foundation under grant CNS-0954039 (CAREER) and Singapore's Agency for Science, Technology and Research (A*STAR) under the Human Sixth Sense Programme.

fusion algorithms. Our analyses are verified through extensive simulations based on both synthetic data sets and data traces collected in a real deployment for vehicle detection.

Key words: Coverage, target detection, data fusion, performance limit

1 Introduction

Recent years have witnessed the deployments of wireless sensor networks (WSNs) for many critical applications such as security surveillance [20], environmental monitoring [30], and target detection/tracking [26]. Many of these applications involve a large number of sensors distributed in a vast geographical area. As a result, the cost of deploying these networks into the physical environment is high. A key challenge is thus to predict and understand the expected sensing performance of these WSNs. A fundamental performance measure of WSNs is *coverage* that characterizes how well a sensing field is monitored by a network. The coverage of a network has two facets, *i.e.*, *spatial coverage* and *temporal coverage*. The spatial coverage quantifies the percentage of area that is well monitored by the network. The temporal coverage quantifies the timeliness of the network in detecting targets appearing in the sensing field. Many recent studies are focused on analyzing the spatiotemporal coverage performance of large-scale WSNs [4, 23, 46, 38, 52, 50, 29].

Despite the significant progress, a key challenge faced by the research on spatiotemporal coverage is the obvious discrepancy between the advanced information processing schemes adopted by existing sensor networks and the overly simplistic sensing models widely assumed in the previous analytical studies. On the one hand, many WSN applications are designed based on *collaborative* signal processing algorithms that improve the sensing performance of a network by jointly processing the noisy measurements of multiple sensors. In practice, various stochastic *data fusion* schemes have been employed by sensor network systems for event monitoring, detection, localization, and classification [20, 26, 14, 13, 10, 39, 25, 34]. On the other hand, collaborative signal processing algorithms such as data fusion often have complex complications to the network-level sensing performance such as coverage. As a result, most analytical studies on spatiotemporal coverage are conducted based on *overly simplistic* sensing models [4, 3, 47, 18, 29, 23, 46, 38, 52, 22, 28]. In particular, the sensing region of a sensor is often modeled as a disc with radius r centered at the position of the sensor, where r is referred to as the *sensing range*. A sensor *deterministically* detects the targets (events) within its sensing range. In Section 2, we will briefly survey the studies that are based on this disc model. Although such a model allows a geometric treatment to the coverage problem, it fails to capture the stochastic nature of sensing.

To illustrate the inaccuracy of the disc sensing model, we plot the sensing performance of an acoustic sensor in Fig. 1 using the data traces collected from a real vehicle detection experiment [14]. In the experiment, the sensor detects moving ve-

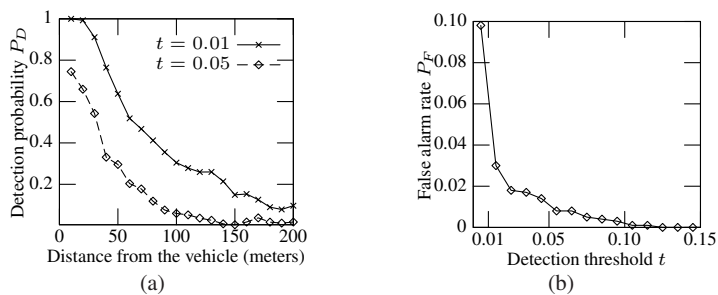


Fig. 1 Sensing performance of an acoustic sensor in detecting vehicle. (a) Detection probability vs. the distance from the vehicle; (b) False alarm rate vs. detection threshold.

hicles by comparing its signal energy measurement against a threshold (denoted by t). Fig. 1(a) plots the probability that the sensor detects a vehicle (denoted by P_D) versus the distance from the vehicle. No clear cut-off boundary between successful and unsuccessful sensing of the target can be seen in Fig. 1(a). Similar result is observed for the relationship between the sensor's false alarm rate (denoted by P_F) and the detection threshold shown in Fig. 1(b). Note that P_F is the probability of making a positive decision when *no* vehicle is present.

In this work, we develop an analytical framework to explore the fundamental limits of spatiotemporal coverage of large-scale WSNs based on stochastic data fusion models. To characterize the inherent stochastic nature of sensing, we propose new measures for quantifying spatiotemporal coverage. Specifically, the *spatial coverage* is defined as the fraction of area in which the target can be detected with a false alarm rate of at most α and a detection probability of at least β . Similarly, to quantify the fundamental trade-off between detection delay and false alarm rate, we propose a new metric called α -delay that is defined as the delay of detecting a target subject to the false alarm rate bound α . The *temporal coverage* is then defined as the reciprocal of α -delay. Compared with the classical definitions of spatial and temporal coverage, these new definitions explicitly capture the performance requirements imposed by sensing applications. For instance, the full spatial coverage of a region with $\alpha = 5\%$ and $\beta = 90\%$ ensures that the probability of detecting any event occurring in the region is no lower than 90% and no more than 5% of the network reports are false alarms. Moreover, in the asymptotic case where α -delay is minimized, any target can be detected almost surely once after its appearance, while the false alarm rate is no greater than α .

The main focus of this paper is to investigate the fundamental scaling laws between spatiotemporal coverage, network density, and signal-to-noise ratio (SNR). To the best of our knowledge, this work is the first to study the spatiotemporal coverage performance of large-scale WSNs based on collaborative sensing models. Our results not only help understand the limitations of the existing analytical results based on the disc model but also provide key insights into designing and

analyzing the large-scale WSNs that adopt stochastic fusion algorithms. The main contributions of this work are as follows:

- We derive the spatiotemporal coverage of random networks under both data fusion and probabilistic disc models. The existing analytical results based on the classical disc model can be naturally extended to the context of stochastic event detection. With these results, we can compute the minimum network density before the deployment or turn on the fewest sensors of an existing network to achieve a desired level of spatiotemporal coverage.
- We study the fundamental scaling laws of spatiotemporal coverage. Let ρ_d and ρ_f denote the minimum network densities for achieving full spatial coverage or minimum detection delay under the disc and fusion models, respectively. For randomly deployed networks, we prove that $\rho_f = \mathcal{O}(\frac{2r^2}{R^2} \cdot \rho_d)$ where r is the radius of sensing disc and R is the fusion range within which the measurements of all sensors are fused. As fusion range can be much greater than sensing range, ρ_f is much smaller than ρ_d . This result shows that data fusion can effectively reduce the network density compared with the disc model. Furthermore, the existing analytical results based on the disc model significantly overestimate the network density required for achieving coverage.
- We study the impact of SNR on the network density when full spatial coverage or minimum detection delay is required. For randomly deployed networks, we prove that $\frac{\rho_f}{\rho_d} = \mathcal{O}(\delta^{2/k})$, where δ is SNR and k is the signal's path loss exponent that typically ranges from 2.0 to 5.0. This result suggests that data fusion is more effective in reducing the density of low-SNR network deployments, while the disc model is suitable only when the SNR is sufficiently high.
- To verify our analyses, we conduct extensive simulations based on both synthetic data sets and real data traces collected from 20 sensors. The simulation results validate our analytical results under a variety of realistic settings.

This chapter is organized as follows. Section 2 reviews the related literature on spatiotemporal coverage and detection delay. Section 3 introduces background and Section 4 derives the spatiotemporal coverage of WSNs. Section 5.1 and Section 5.2 study the impact of data fusion on spatial and temporal coverage, respectively. Section 6 discusses the implications of results and several open issues. Section 7 presents the results of performance evaluation. Section 8 concludes this chapter.

2 Related Work

2.1 Coverage

As one of the most fundamental issues in WSNs, the coverage problem has attracted significant research attention. Previous works fall into two categories, namely, theoretical analysis of coverage performance and coverage maintenance algorithms/protocols.

These two categories are reviewed briefly as follows, respectively. As this chapter falls into the category of the theoretical analysis of coverage performance, our review will be mainly focused on this category.

2.1.1 Analysis of Coverage

Theoretical studies of the coverage of large-scale WSNs have been conducted in [4, 29, 23, 18, 46, 38, 52, 22, 28]. Most works [23, 46, 38, 52, 22, 28] focus on deriving the asymptotic coverage of WSNs. The k -coverage is a coverage model widely used in these studies. Specifically, a network provides k -coverage if any physical point is within the sensing range of at least k sensors.

Kumar *et al.* [23] consider duty-cycled WSNs that are deployed on a $\sqrt{n} \times \sqrt{n}$ grids, random uniform and Poisson with density n . Each sensor independently sleeps in each time slot with probability of p . They prove that the critical value of the function $np\pi r^2 / \log(np)$ is 1 for the event of k -coverage, where r is the sensor's sensing range. In other words, when the network size n increases, to ensure k -coverage, r has an asymptotic lower bound of $\sqrt{\frac{\log np}{np}}$.

Wan *et al.* [46] assume that the sensors are deployed as either a Poisson point process or a uniform point process in a square or disk region. They study two asymptotic scaling laws: (i) how the probability of k -coverage changes with the sensing range and the number of sensors, when the region to be covered is a unit square or disk; and (ii) how the probability of k -coverage changes with the area of the region to be covered and the number of sensors, when the sensors have unit sensing range. The upper and lower bounds for the probability of k -coverage are derived. Moreover, the asymptotic conditions for the k -coverage with high probability are also derived.

Shakkottai *et al.* [38] consider that n sensors are deployed at the grid points of a unit square area. They prove the necessary and sufficient conditions for the 1-coverage and network connectivity, *i.e.*, $p \cdot r$ has an order of $\frac{\log n}{n}$, where p is the probability that a sensor is active. They also derive the order of the number of hop counts from any active node to another, which is $\sqrt{n/\log n}$. This study assumes that the sensing range and communication range are the same, which is a limitation of this study.

Zhang *et al.* [52] consider a Poisson sensor deployment with density λ in a square region with side length l , where each sensor covers a unit disk. They derive the necessary and sufficient condition of λ for k -coverage when l increases, *i.e.*, $\lambda = \log l^2 + (k+1) \log \log l^2 + c(l)$ where $c(l) \rightarrow +\infty$ as $l \rightarrow \infty$. Based on this result, they prove that the upper bound of the network lifetime is kT where T is the lifetime of a single sensor, if $\lambda = \log l^2 + (k+1) \log \log l^2 + c(l)$ where $c(l) \rightarrow -\infty$ as $l \rightarrow \infty$.

The above studies [23, 46, 38, 52] focus on the full k -coverage over all region, *i.e.*, every physical point is covered by at least k sensors. In [22], Kumar *et al.* study the k -barrier coverage problem: when an intruder crosses a belt area deployed with sensors, it can be detected with high probability by at least k sensors. Different from the full k -coverage, k -barrier coverage does not require that each physical

point in the monitored region is covered by k sensors. If sensors are stealthy, the k -barrier coverage is defined as *weak* k -barrier coverage; otherwise, it is defined as *strong* k -barrier coverage. The critical conditions for *weak* and *strong* k -barrier coverage are derived by Kumar *et al.* in [22] and Liu *et al.* in [28], respectively. The critical conditions can be used to compute the minimum number of sensors to provide barrier coverage with high probability.

Ammari *et al.* [2] study the critical phase transitions for coverage and connectivity based on percolation theory. Specifically, the sensing-coverage phase transition is the abrupt change from small fragmented covered areas to a single large covered area, when more sensors are continuously added to a WSN. Similarly, the network-connectivity phase transition is the abrupt change from an originally disconnected WSN to a connected WSN as more sensors are added. The covered area fractions for both transitions are derived at critical percolation.

Liu *et al.* [29] study the coverage performance of WSNs using other three coverage metrics, *i.e.*, area coverage, node coverage, and detectability. The area coverage is defined as the fraction of the geographical area covered by one or more sensors. The node coverage is defined as the fraction of sensors that can be removed without reducing the area coverage. Detectability is defined as the probability that a WSN can detect an object moving along a line segment in the WSN. Liu *et al.* derive the closed-form formulas of these three coverage metrics for random infinite plane deployments and random strip deployments under the disc sensing model and a general sensing model that considers signal decay, respectively.

The temporal coverage, *i.e.*, the latency of detecting a target, is another important facet of the coverage performance of WSNs. Cao *et al.* [5] derive the average latencies of detecting static or mobile target when sensors are deployed randomly and follow a random sleep scheduling scheme. Dousse *et al.* [12] address a similar problem where only the sensors with a connected path to the sink are considered. In [24], Lazos *et al.* map the problem of detecting mobile targets using randomly deployed sensors to a line-set intersection problem. Their analysis shows that the detection probability and the detection delay depends on the length of the perimeters of the sensing areas of sensors and not their shapes.

Most of the above theoretical results on coverage for both static and mobile sensors/targets are surveyed and compared in [4]. However, all the above theoretical studies are based on the deterministic disc model. In this chapter, we compare our results obtained under a data fusion model against the results from [29, 4].

2.1.2 Coverage Maintenance Algorithms

Early work [31, 27, 32] quantifies spatiotemporal coverage by the length of target's path where the accumulative observations of sensors are maximum or minimum [31, 27, 32]. However, these works focus on devising algorithms for finding the target's paths with certain level of coverage. Several algorithms and protocols [7, 50, 51] are designed to maintain spatiotemporal coverage using the minimum number of sensors. However, the effectiveness of these schemes largely relies

on the assumption that sensors have circular sensing regions and deterministic sensing capability. Several recent studies [21, 37, 1, 48, 53] on the coverage problem have adopted probabilistic sensing models. The numerical results in [48] show that the coverage of a network can be expanded by the cooperation of sensors through data fusion. However, these studies do not quantify the improvement of coverage due to data fusion techniques. Different from our focus on analyzing the fundamental limits of coverage in WSNs, all of these studies aim to devise algorithms and protocols for coverage maintenance.

2.2 Data Fusion

There is a vast of literature on stochastic signal detection based on multi-sensor data fusion. Early works [6, 44] focus on small-scale powerful sensor networks (*e.g.*, several radars). Recent studies on data fusion have considered the specific properties of WSNs such as sensors' spatial distribution [13, 14, 34] and limited sensing/communication capability [10]. However, these studies focus on analyzing the optimal fusion strategies that maximize the system performance of a given network. In contrast, this chapter explores the fundamental limits of spatiotemporal coverage of WSNs that are designed based on existing data fusion strategies. Recently, irregular sampling theory has been applied for reconstructing physical fields in WSNs [36, 35]. Different from these works that focus on developing sampling schemes to improve the quality of signal reconstruction, we aim to analyze sensors' spatial density for achieving the required level of coverage.

Many sensor network systems have incorporated various data fusion schemes to improve the system performance. In the surveillance system based on MICA2 motes [20], the system false alarm rate is reduced by fusing the detection decisions made by multiple sensors. In the DARPA SensIT project [14], advanced data fusion techniques have been employed in a number of algorithms and protocols designed for target detection [26, 10], localization [39, 25], and classification [13, 14]. Despite the wide adoption of data fusion in practice, the performance analysis of large-scale fusion-based WSNs has received little attention.

3 Preliminaries and Problem Definition

This section first introduces the preliminaries in Section 3.1, and then formally defines the spatiotemporal coverage of wireless sensor networks in Section 3.2.

3.1 Preliminaries

In this section, we describe the technical preliminaries of this chapter, which include sensor measurement, network and data fusion models.

3.1.1 Sensor Measurement Model

We assume that sensors perform detection by measuring the energy of signals emitted by the target.¹ The energy of most physical signals (*e.g.*, acoustic and electromagnetic signals) attenuates with the distance from the signal source. Suppose sensor i is d_i meters away from the target that emits a signal of energy S_0 . The attenuated signal energy s_i at the position of sensor i is given by $s_i = S_0 \cdot w(d_i)$, where $w(\cdot)$ is a decreasing function satisfying $w(0) = 1$, $w(\infty) = 0$, and $w(x) = \Theta(x^{-k})$. The $w(\cdot)$ is referred to as the *signal decay function*. Depending on the environment, *e.g.*, atmosphere conditions, the signal's path loss exponent k typically ranges from 2.0 to 5.0 [25, 19]. We note that the theoretical results derived in this chapter do not depend on the closed-form formula of $w(\cdot)$. We adopt the following signal decay function in the simulations conducted in this chapter:

$$w(x) = \frac{1}{1 + x^k}. \quad (1)$$

The sensor measurements are contaminated by additive random noises from sensor hardware or environment. Depending on the hypothesis that the target is absent (H_0) or present (H_1), the measurement of sensor i , denoted by y_i , is given by

$$H_0 : y_i = n_i, \quad H_1 : y_i = s_i + n_i,$$

where n_i is the energy of noise experienced by sensor i . We assume that the noise n_i at each sensor i follows the normal distribution, *i.e.*, $n_i \sim \mathcal{N}(\mu, \sigma^2)$, where μ and σ^2 are the mean and variance of n_i , respectively. We assume that the noises, $\{n_i | \forall i\}$, are spatially independent across sensors. Therefore, the noises at sensors are independent and identically distributed (*i.i.d.*) Gaussian noises. In the presence of target, the measurement of sensor i follows the normal distribution, *i.e.*, $y_i | H_1 \sim \mathcal{N}(s_i + \mu, \sigma^2)$. Due to the independence of noises, the sensors' measurements, $\{y_i | \forall i, H_1\}$, are spatially independent but *not* identically distributed as sensors receive different signal energies from the target. We define the peak signal-to-noise ratio (PSNR) as $\delta = S_0/\sigma$ which quantifies the noise level. The symbols used in this chapter are summarized in Table 1.

The above signal decay and additive *i.i.d.* Gaussian noise models have been widely adopted in the literature of multi-sensor signal detection [44, 10, 39, 25,

¹ Several types of sensors (*e.g.*, acoustic sensor) only sample *signal intensity* at a given sampling rate. The *signal energy* can be obtained by preprocessing the time series of a given interval, which has been commonly adopted to avoid the transmission of raw data [14, 13, 10, 39, 25].

Table 1 Summary of Notation*

Symbol*	Definition
$\mathcal{O}(\cdot)$	asymptotic upper bound notation
$\Theta(\cdot)$	asymptotic tight bound notation
$Q(x)$	CCDF of standard normal distribution
S_0	original signal energy emitted by the target
μ, σ^2	mean and variance of noise energy
δ	PSNR, $\delta = S_0/\sigma$
k	path loss exponent
$w(\cdot)$	signal decay function, $w(x) = \Theta(x^{-k})$
s_i	attenuated signal energy
n_i	noise energy, $n_i \sim \mathcal{N}(\mu, \sigma^2)$
y_i	signal energy measurement, $y_i = s_i + n_i$
Y	fusion statistic at cluster head / base station
P_F / P_D	false alarm rate / detection probability
α / β	upper / lower bound of P_F / P_D
H_0 / H_1	hypothesis that the target is absent / present
ρ	network density
$\mathbf{F}(p)$	the set of sensors within fusion range of point p
$N(p)$	the number of sensors in $\mathbf{F}(p)$
ϵ	upper bound of target localization error
t	local detection threshold
T	detection threshold at cluster head
T_D	detection period
R	fusion range under data fusion model
r	disc radius under disc sensing model
c	spatial coverage of a network
τ	average detection delay of a network
v	movement speed of target

* The symbols with subscript i refer to the notation of sensor i .

34, 6, 48, 29, 32, 1] and also have been empirically verified [19, 25]. In practice, the parameters of these models (*i.e.*, S_0 , $w(\cdot)$, μ , and σ^2) can be estimated using the training data collected by the existing WSN or several *in situ* sensors before the large-scale deployment. The normal distribution might be an approximation to the real noise distribution in practice. As discussed in Section 6.2, the assumption of *i.i.d.* Gaussian noises can be relaxed to any *i.i.d.* noises.

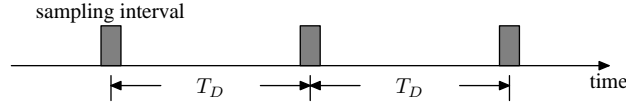


Fig. 2 Temporal view of a single sensor's operation. The sensor outputs an energy measurement after each sampling interval.

3.1.2 Network Model

We consider a network deployed in a vast two-dimensional geographical region. The positions of sensors are uniformly and independently distributed in the region. Such a deployment scenario can be modeled as a stationary two-dimensional Poisson point process. Let ρ denote the density of the underlying Poisson point process. The number of sensors located in a region A , $N(A)$, follows the Poisson distribution with mean of $\rho||A||$, *i.e.*, $N(A) \sim \text{Poi}(\rho||A||)$, where $||A||$ represents the area of the region A . We note that the uniform sensor distribution has been widely adopted in the performance analysis of large-scale WSNs [4, 23, 46, 38, 29]. Therefore, this assumption allows us to compare our results with previous analytical results.

When we analyze the temporal coverage performance of a network, we consider the following sensor sampling scheme and target mobility model. We assume that a sensor executes detection task every T_D seconds. T_D is referred to as the *detection period*. In each detection period, a sensor gathers the signal energy during the *sampling interval* for the detection made in the current detection period. We assume that the sampling interval is much shorter than the detection period. The temporal view of a single sensor's operation is illustrated in Fig. 2. We note that such an intermittent measurement scheme is consistent with several wireless sensor systems for target detection and tracking [20, 13, 14]. For instance, a sensor may wake up every 5 seconds and sample acoustic energy for 0.05 seconds, where T_D is 5 s and the sampling interval is 0.05 s [14]. We assume that the target may appear at any location in the deployment region and move freely. Moreover, the target is blind to the network, *i.e.*, the target does not know the sensors' positions, and hence it cannot choose a movement scheme to reduce the probability of being detected. The sensors synchronously detect the target, and we refer to the target detection in one detection period as the *unit detection*. The process of detecting a target consists of a series of unit detections. As the sampling interval is much shorter than the detection period, we ignore the target's movement during the sampling interval.

3.1.3 Data Fusion Model

Data fusion can improve the performance of detection systems by jointly considering the noisy measurements of multiple sensors. There exist two basic data fusion schemes, namely, *decision fusion* and *value fusion*. In decision fusion, each sensor makes a *local* decision based on its measurements and sends its decision to the cluster head, which makes a *system* decision according to the local decisions. In value

fusion, each sensor sends its measurements to the cluster head, which makes the detection decision based on the received measurements. In this chapter, we focus on value fusion, as it usually has better detection performance than decision fusion [44]. Most of the results in this chapter can be extended to address the decision fusion model. The details of the extensions can be found in [42, 41]. The optimal value fusion rule is to compare a weighted sum of sensors' measurements, *i.e.*, $\sum_i \frac{s_i}{\sigma} \cdot y_i$, to a threshold [41]. However, as sensor measurements contain both noise and signal energy, the weight $\frac{s_i}{\sigma}$, *i.e.*, the SNR received by sensor i , is unknown. A practical solution is to adopt equal constant weights for all sensors' measurements [34, 10, 48]. Since the measurements from different sensors are treated equally, the sensors far away from the target should be excluded from data fusion as their measurements suffer low SNRs. Therefore, we adopt a fusion scheme as follows.

When the network detects whether a target is present at a physical point p , the sensors within a distance of R meters from p form a cluster and fuse their measurements to detect whether a target is present at p . R is referred to as the *fusion range* and $\mathbf{F}(p)$ denotes the set of sensors within the fusion range of p . The number of sensors in $\mathbf{F}(p)$ is represented by $N(p)$. A cluster head is elected to make the detection decision by comparing the sum of measurements reported by member sensors in $\mathbf{F}(p)$ against a detection threshold T . Let Y denote the *fusion statistic*, *i.e.*, $Y = \sum_{i \in \mathbf{F}(p)} y_i$. If $Y \geq T$, the cluster head decides H_1 ; otherwise, it decides H_0 .

We assume that the cluster head makes a detection based on snapshot measurements from member sensors in each unit detection without using temporal samples to refine the detection decision. Such a snapshot scheme is widely adopted in previous works on target surveillance [10, 39, 25, 34, 48]. Fusion range R is an important design parameter of our data fusion model. As SNR received by sensor decays with distance from the target, fusion range lower-bounds the quality of information that is fused at the cluster head. The above data fusion model is consistent with the fusion schemes adopted in [34, 10, 48]. If more efficient fusion models are employed, the scaling laws proved in this chapter still hold as discussed in Section 6.2. When the network is requested to detect whether a target is present at a specified position, a cluster forms around the specified position. When the target position is not specified, we assume that the target position can be obtained through a localization algorithm. For instance, the target position can be estimated as the geometric center of a number of sensors with the largest measurements. Such a simple localization algorithm is employed in the simulations conducted in this chapter. The localized position may not be the exact target position and the distance between them is referred to as *localization error*. We assume that the localization error is upper-bounded by a constant ϵ . The localization error is accounted for in the following analyses. However, we show that it has no impact on the asymptotic results derived in this chapter. When the target is absent and the network is requested to make a detection, a cluster will still be formed and most likely yield a negative detection decision.

The above data fusion model can be used for target detection as follows. The detection can be triggered by user queries or executed periodically. In a detection process, each sensor makes a snapshot measurement and a cluster is formed by

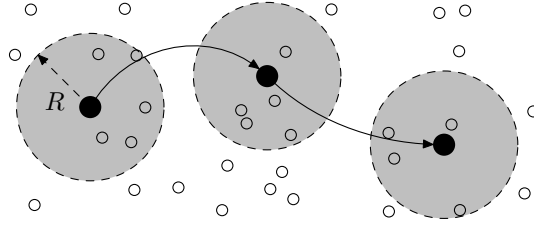


Fig. 3 Target detection under data fusion model. The void circles represent randomly deployed sensors; the solid circles represent the target in different sampling intervals, and a unit detection is performed in each sampling interval; the dashed discs represent the fusion ranges.

the sensors within the fusion range from the possible target to make a detection decision. The cluster formation may be initiated by the sensor that has the largest measurement. Such a scheme can be implemented by several dynamic clustering algorithms [8]. Fig. 3 illustrates the intrusion detection under the data fusion model. The fusion range R can be used as an input parameter of the clustering algorithm. The communication topology of the cluster can be a multi-hop tree rooted at the cluster head. As the fusion statistic Y is an aggregation of sensors' measurements, it can be computed efficiently along the routing path to the cluster head. In this chapter, we are interested in the fundamental performance limits of spatial and temporal coverage under the fusion model and the design of clustering and data aggregation algorithms is beyond the scope of this chapter.

3.2 Definitions and Problem Statement

3.2.1 Definition of Spatiotemporal Coverage

The detection of a target is inherently stochastic due to the noise in sensor measurements. The detection performance is usually characterized by two metrics, namely, the false alarm rate (denoted by P_F) and detection probability (denoted by P_D). P_F is the probability of making a positive decision when *no* target is present, and P_D is the probability that a present target is correctly detected. In stochastic detection, positive detection decisions may be false alarms caused by the noise in sensor measurements. In particular, although the detection probability can be improved by setting lower detection thresholds, the fidelity of detection results may be unacceptable because of high false alarm rates. Therefore, P_F together with P_D characterize the sensing quality provided by the network. For a physical point p , we denote the probability of successfully detecting a target located at p as $P_D(p)$. Note that P_F is the probability of making positive decision when *no* target is present, and hence is location independent. We first introduce a concept called (α, β) -covered.

Definition 1 ((α, β) -covered). Given two constants $\alpha \in (0, 0.5)$ and $\beta \in (0.5, 1)$, a physical point p is (α, β) -covered if the false alarm rate P_F and detection probability

$P_D(p)$ satisfy

$$P_F \leq \alpha, \quad P_D(p) \geq \beta.$$

We now formally define *spatial coverage* that quantifies the fraction of the surveillance region where P_F and P_D are bounded by α and β , respectively.

Definition 2 (Spatial coverage). The spatial coverage of a region is defined as the fraction of points in the region that are (α, β) -covered.

There also exists a fundamental trade-off between the delay of detection and false alarm rate. Although detection delay can be reduced by making sensors more sensitive (*e.g.*, setting lower detection threshold), the fidelity of detection results may be unacceptable due to high false alarm rates. Therefore, studying detection delay alone without the consideration of false alarm is meaningless. We now introduce a new concept called α -delay that quantifies the delay of detection under bounded false alarm rate.

Definition 3 (α -delay). α -delay is the average number of detection periods before a target is first detected subject to that the false alarm rate of the network is no greater than α , *i.e.*, $P_F \leq \alpha$, where $\alpha \in (0, 1)$.

We now formally define *temporal coverage* that quantifies the timeliness of the network in detecting targets under bounded false alarm rate.

Definition 4 (Temporal coverage). Temporal coverage is the reciprocal of α -delay.

In addition, we define the following terminologies. The *full spatial coverage* of a region refers to the case where the spatial coverage of the region approaches one, *i.e.*, the false alarm rate is below α and the probability of detecting a target present at *any* location is above β . The *instant detection* refers to the case where the α -delay or temporal coverage approaches one, *i.e.*, any target can be detected almost surely in the first detection period after its appearance while the system false alarm rate is below α . In practice, mission-critical surveillance applications [20, 16, 14, 17] require that the target can be detected with a high detection probability while the network maintains a low false alarm rate. Therefore, we can set α and β accordingly to meet these requirements.

We now illustrate the spatial coverage by an example, where PSNR $\delta = 1000$ (*i.e.*, 30 dB), $\alpha = 5\%$, $\beta = 95\%$, and $R = 50$ m. Fig. 4(a) and 4(b) illustrate the spatial coverage under the disc and fusion models, respectively. In Fig. 4(b), when a target (represented by the triangle) is present, the sensors within the fusion range from it fuse their measurements to make a detection. The gray area is (α, β) -covered, where grayscale represents the value of P_D at each point. As shown in Fig. 4(a), the covered region under the disc model is simply the union of all sensing discs. As a result, when a high level of spatial coverage is required, a large number of extra sensors must be deployed to eliminate small uncovered areas surrounded by sensing discs. In contrast, data fusion can effectively expand the covered region by exploiting the collaboration among neighboring sensors.

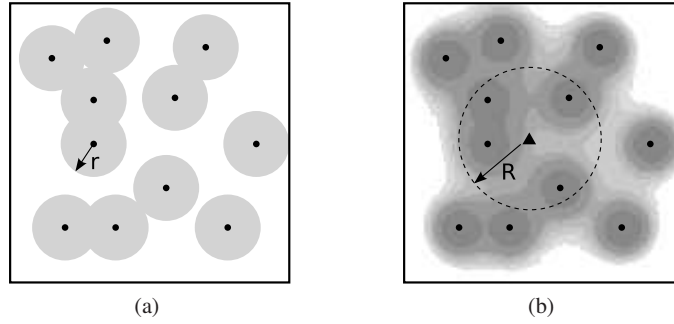


Fig. 4 Spatial coverage. (a) Spatial coverage under the disc model. Sensing range $r = 17$ m, which is computed by (4). (b) Spatial coverage under the fusion model. Grayscale represents the value of P_D .

3.2.2 Problem Statement

In the rest of this chapter, we consider the following problems:

1. Although a number of analytical results on spatiotemporal coverage [4, 23, 46, 38, 52, 50, 51, 29, 5, 12, 24, 3] have been obtained under the classical disc model, are they still applicable under the probabilistic definition spatiotemporal coverage which explicitly captures the stochastic nature of sensing? To answer this question, we propose a probabilistic disc model such that the existing results can be naturally extended to the context of stochastic detection (Section 4.1).
2. How to quantify the spatiotemporal coverage when sensors can collaborate through data fusion? Answering this question enables us to evaluate the spatiotemporal coverage performance of a network. Moreover, it allows us to deploy the fewest sensors for achieving a given level of spatiotemporal coverage (Sections 4.2).
3. What are the scaling laws between spatiotemporal coverage, network density, and SNR under both the disc and fusion models? The results will provide important insights into understanding the limitation of analytical results based on the disc model as well as the impact of data fusion on the detection performance of large-scale WSNs (Sections 5).

4 Spatiotemporal Coverage of Wireless Sensor Networks

In this section, we derive the spatiotemporal coverage of large-scale WSNs under the disc model and the data fusion model, in Section 4.1 and Section 4.2, respectively.

4.1 Spatiotemporal Coverage under Probabilistic Disc Model

As the classical disc model deterministically treats the detection performance of sensors, existing results based on this model [4, 23, 46, 38, 52, 50, 51, 29, 5, 12, 24, 3] cannot be readily applied to analyze the performance or guide the design of real-world WSNs. In this section, we extend the classical disc model based on the stochastic detection theory [44] to capture several realistic sensing characteristics and study the spatiotemporal coverage under the extended model. The extended results will be used as the baselines to study the impact of data fusion on the sensing performance of WSNs.

4.1.1 Probabilistic Disc Model

In the *probabilistic disc model*, we choose the sensing range r such that 1) the probability of detecting any target within the sensing range is no lower than β , and 2) the false alarm rate is no greater than α . As we ignore the detection probability outside the sensing range of a sensor, the detection capability of sensor under this model is lower than in reality. However, this model preserves the *boundary* of sensing region defined in the classical disc model. Hence, the existing results based on the classical disc model [4, 23, 46, 38, 52, 50, 51, 29, 5, 12, 24, 3] can be naturally extended to the context of stochastic detection.

We now discuss how to choose the sensing range r under the probabilistic disc model. The optimal Bayesian detection rule for a single sensor i is to compare its measurement y_i to a detection threshold t [44]. If y_i exceeds t , sensor i decides H_1 ; otherwise, it decides H_0 . Hence, the false alarm rate P_F and detection probability P_D of sensor i are given by

$$P_F = \mathbb{P}(y_i \geq t | H_0) = Q\left(\frac{t - \mu}{\sigma}\right), \quad (2)$$

$$P_D = \mathbb{P}(y_i \geq t | H_1) = Q\left(\frac{t - \mu - s_i}{\sigma}\right), \quad (3)$$

where $\mathbb{P}(\cdot)$ is the probability notation and $Q(\cdot)$ is the complementary cumulative distribution function (CCDF) of the standard normal distribution, *i.e.*, $Q(x) = \frac{1}{\sqrt{2\pi}} \int_x^\infty e^{-t^2/2} dt$. As P_D is non-decreasing function of P_F [44], it is maximized when P_F is set to be the upper bound α . Hence the optimal detection threshold can be solved from (2) as $t_{\text{opt}} = \mu + \sigma Q^{-1}(\alpha)$, where $Q^{-1}(\cdot)$ is the inverse function of $Q(\cdot)$. By replacing $t = t_{\text{opt}}$ and $s_i = S_0 \cdot w(r)$ in (3), we have

$$r = w^{-1}\left(\frac{Q^{-1}(\alpha) - Q^{-1}(\beta)}{\delta}\right), \quad (4)$$

where $w^{-1}(\cdot)$ is the inverse function of $w(\cdot)$. If the target is more than r meters from the sensor, the detection performance requirements, *i.e.*, α and β , cannot be

satisfied by setting any detection threshold. Note that a similar definition of sensing range is proposed in [48] for stochastic detection. From (4), the sensing range of a sensor varies with the user requirements (*i.e.*, α and β) and PSNR δ . For instance, the sensing range r is 3.8 m if $\alpha = 5\%$, $\beta = 95\%$, $\delta = 50$ (*i.e.*, 17 dB) and $w(\cdot)$ is given by (1) with $k = 2$. Note that the PSNR of 17 dB is set according to the measurements from the vehicle detection experiments based on MICA2 [16] and ExScal [17] motes. As $w(\cdot)$ is a decreasing function, $w^{-1}(\cdot)$ is also a decreasing function. Therefore, r increases with the PSNR δ according to (4). This conforms to the intuition that a sensor can detect a farther target if the noise level is lower (*i.e.*, a greater δ).

4.1.2 Spatial Coverage under Probabilistic Disc Model

We now extend the spatial coverage of random networks [29, 4] derived under the classical disc model to probabilistic disc model. Under both the classical and probabilistic disc models, a location is regarded as being covered if it is within at least one sensor's sensing range. Accordingly, the area of the union of all sensors' sensing ranges is regarded as being covered by the network. The coverage of random networks under the classical disc model has been extensively studied based on the stochastic geometry theory [29, 4]. The results [29, 4] can be stated as the following lemma:

Lemma 1. *Let c denote the spatial coverage under the disc model, we have*

$$c = 1 - e^{-\rho\pi r^2}, \quad (5)$$

where ρ is the network density.

If the sensing range r is chosen by (4), Eq. (5) computes the spatial coverage of a random network under the probabilistic disc model. This result will be used as the basis for studying the impact of data fusion on spatial coverage in Section 5.1.

4.1.3 Temporal Coverage under Probabilistic Disc Model

Before deriving the temporal coverage under probabilistic disc model, we first introduce the target detection under the model. The network periodically detects the target as described in Section 3.1.2. In each unit detection, if the target is within at least one sensor's sensing range, the target is detected with a probability no lower than β . We let β be sufficiently close to 1 (*e.g.*, $\beta = 0.99$) such that the target is detected almost surely if it is within any sensor's sensing range. Such a setting enables the sensors to exhibit similar deterministic property as under the classical disc model. We refer to the circular region with radius of r centered at the target as the *target disc*. Hence, the target is detected if there is at least one sensor within the target disc. In this section, we assume that there is no overlap between any two target discs

such that the unit detections are independent from each other. Such independence among unit detections can significantly simplify the analysis. In Section 5.2.2, we will extend the analysis to the case where target discs may overlap. We now discuss the condition for no overlap between any two target discs. Suppose the target moves at a constant speed of v , the no-overlap condition can be satisfied if $vT_D > 2r$. For instance, if the sensing range r is 3.8 m as mentioned in Section 4.1.1 and the target speed v is 5 m/s (*i.e.*, 18 km/h) [14], the target discs will no overlap as long as the detection period T_D is greater than 2 s. We have the following lemma. The proof can be found in Appendix 1.

Lemma 2. *Let τ denote the α -delay under the probabilistic disc model. If there is no overlap between any two target discs,*

$$\tau = \frac{1}{1 - e^{-\rho\pi r^2}}.$$

We can see from Lemma 2 that the α -delay decreases with network density ρ and sensing range r . Note that r is given by (4) under the probabilistic disc model. With the α -delay, we can calculate the temporal coverage of the network.

4.2 Spatiotemporal Coverage under Data Fusion Model

Although the probabilistic disc model discussed in Section 4.1 captures the stochastic nature of sensing, it does not exploit the collaboration among sensors. In this section, we first derive the spatiotemporal coverage of random networks under the fusion model and illustrate the analytical results using numerical examples.

4.2.1 Spatial Coverage under Data Fusion Model

We have the following lemma regarding the spatial coverage of random networks. The proof can be found in Appendix 2.

Lemma 3. *The spatial coverage of a uniformly deployed network under the data fusion model, denoted by c , is*

$$c = \mathbb{P} \left(\frac{\sum_{i \in \mathbf{F}(p)} s_i}{\sqrt{N(p)}} \geq \sigma (Q^{-1}(\alpha) - Q^{-1}(\beta)) \right), \quad (6)$$

where p is an arbitrary physical point in the network.

As p is an arbitrary point in the network, $N(p)$ is a Poisson random variable, *i.e.*, $N(p) \sim \text{Poi}(\rho\pi R^2)$. Moreover, $\{s_i | i \in \mathbf{F}(p)\}$ are also random variables. However, we have no closed-form formula for computing (6) due to the difficulty of deriving

the cumulative distribution function (CDF) of $\frac{\sum_{i \in \mathbf{F}(p)} s_i}{\sqrt{N(p)}}$. We now give an approximation to (6) in the following lemma. The proof can be found in Appendix 3.

Lemma 4. *Let μ_s and σ_s^2 denote the mean and variance of $s_i | i \in \mathbf{F}(p)$ for arbitrary point p , respectively. The spatial coverage of a uniformly deployed network under the data fusion model can be approximated by*

$$c \simeq Q \left(\frac{\gamma(R) - \rho\pi R^2}{\sqrt{\rho\pi R^2}} \right), \quad (7)$$

$$\text{where } \gamma(R) = \left(\frac{Q^{-1}(\alpha)\sigma - Q^{-1}(\beta)\sqrt{\sigma_s^2 + \sigma^2}}{\mu_s} \right)^2.$$

We note that the formulas of μ_s and σ_s^2 are given by (20) and (21), respectively. As central limit theorem (CLT) is applied in the derivation of (7) (see Appendix 3), this approximation is accurate when $N(p) \geq 20$ [33]. This condition can be easily met in many applications. For example, it is shown in [16] that the detection probability is only about 40% when four MICA2 motes are deployed in a $10 \times 10 \text{ m}^2$ region. Suppose $R = 20 \text{ m}$ and the network density is the same as in [16], $N(p)$ will be about 50. With the approximate formula, we can evaluate the coverage performance of an existing network or compute the minimum network density to achieve the desired level of coverage under the fusion model. Our simulation results in Section 7 show that (7) can provide accurate prediction of coverage under the fusion model. We note that the localization error has little impact on the accuracy of the approximate formula when $R \gg \epsilon$. Recent sensor network localization protocols can achieve a precision within 0.5 m in large-scale outdoor deployments [43].

We now derive the lower bound of spatial coverage under the fusion model, which will be used in the derivations of scaling laws in Section 5.1. We denote $F_{\text{Poi}}(\cdot | \lambda)$ as the CDF of the Poisson distribution $\text{Poi}(\lambda)$, which is formally given by $F_{\text{Poi}}(x | \lambda) = \sum_{k=0}^{\lfloor x \rfloor} \frac{e^{-\lambda} \lambda^k}{k!}$. We have the following lemma. The proof can be found in Appendix 4.

Lemma 5. *The lower bound of spatial coverage of a uniformly deployed network under the data fusion model, denoted by c_L , is given by*

$$c_L = 1 - F_{\text{Poi}}(\Gamma(R) | \rho\pi R^2), \quad (8)$$

where

$$\Gamma(R) = \left(\frac{Q^{-1}(\alpha) - Q^{-1}(\beta)}{\delta} \right)^2 \cdot \frac{1}{w^2(R + \epsilon)}. \quad (9)$$

When $\rho\pi R^2$ is large enough,

$$c_L = Q \left(\frac{\Gamma(R) - \rho\pi R^2}{\sqrt{\rho\pi R^2}} \right). \quad (10)$$

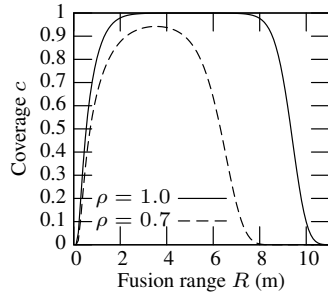


Fig. 5 Spatial coverage vs. fusion range ($\delta = 4$, $\alpha = 5\%$, $\beta = 95\%$).

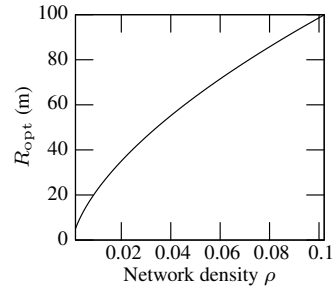


Fig. 6 Optimal fusion range vs. density ($\delta = 100$, $\alpha = 5\%$, $\beta = 95\%$).

We now provide several numerical results to help understand the spatial coverage performance of random networks under the data fusion model. We adopt the signal decay function given by (1) with $k = 2$. Fig. 5 plots the approximate coverage computed by (7). We can see from Fig. 5 that the coverage initially increases with fusion range R , but decreases to zero eventually. Intuitively, as the fusion range increases, more sensors contribute to the data fusion resulting in better sensing quality. However, as R becomes very large, the aggregate noise starts to cancel out the benefit because the target signal decreases quickly with the distance from the target. In other words, the measurements of sensors far away from the target contain low quality information and hence fusing them leads to lower detection performance. An important question is thus how to choose the optimal fusion range (denoted by R_{opt}) that maximizes the coverage. First, the R_{opt} can be obtained through numerical experiments. Fig. 6 plots the optimal fusion ranges under different network densities, which are obtained by numerically maximizing the coverage. Second, it is possible to obtain the analytical R_{opt} by solving $\frac{dc}{dR} = 0$. For instance, when the signal decay function $w(\cdot)$ is given by (1) with $k = 2$, R_{opt} satisfies $\frac{R_{\text{opt}}}{\ln R_{\text{opt}}} = \Theta(\sqrt{\rho})$ and hence R_{opt} increases with network density ρ .

4.2.2 Temporal Coverage under Data Fusion Model

As discussed in Section 3.1.2, sensors perform a unit detection in each detection period and hence the process of detecting a target consists of a series of unit detections. Denote \mathbf{F}_j as the set of sensors within the fusion range in the j th unit detection. Suppose there are N_j sensors in \mathbf{F}_j . When no target is present, we have $Y|H_0 = \sum_{i \in \mathbf{F}_j} n_i \sim \mathcal{N}(N_j\mu, N_j\sigma^2)$, which has been proved in Lemma 3. Therefore, the false alarm rate of the j th unit detection, denoted by P_{F_j} , is given by $P_{F_j} = \mathbb{P}(Y \geq \eta|H_0) = Q\left(\frac{T - N_j\mu}{\sqrt{N_j}\sigma}\right)$, where T is the detection threshold. As P_D is a non-decreasing function of P_F [44], it is maximized when P_F is set to be the upper bound α . Let $P_{F_j} = \alpha$, the optimal detection threshold can be derived

as $T_{\text{opt}} = N_j \mu + \sqrt{N_j} \sigma Q^{-1}(\alpha)$. When the target is present, the sum of energy measurements in the j th unit detection approximately follows a normal distribution $Y|H_1 = \sum_{i \in \mathbf{F}_j} s_i + \sum_{i \in \mathbf{F}_j} n_i \sim \mathcal{N}(N_j \mu_s + N_j \mu, N_j \sigma_s^2 + N_j \sigma^2)$, which has been proved in Lemma 4. The detection probability in the j th unit detection, denoted by P_{Dj} , is given by $P_{Dj} = \mathbb{P}(Y \geq T|H_1) \simeq Q\left(\frac{T - N_j \mu_s - N_j \mu}{\sqrt{N_j \cdot \sqrt{\sigma_s^2 + \sigma^2}}}\right)$. By replacing T with the optimal detection threshold T_{opt} , we have

$$P_{Dj} \simeq Q\left(\frac{\sigma}{\sqrt{\sigma_s^2 + \sigma^2}} \cdot Q^{-1}(\alpha) - \frac{\mu_s}{\sqrt{\sigma_s^2 + \sigma^2}} \cdot \sqrt{N_j}\right). \quad (11)$$

Based on the above performance modeling of each unit detection, we now derive the α -delay under the data fusion model. In this section, we assume that there is no overlap between any two fusion ranges (as shown in Fig. 3). As a result, the sensor sets $\{\mathbf{F}_j | j \geq 1\}$ are independent from each other. Such independence can significantly simplify the analysis. In Section 5.2.2, we extend the analysis to the case where fusion ranges may overlap. We now discuss the condition for no overlap between any two fusion ranges. Suppose the target moves at a constant speed of v , the no-overlap condition can be satisfied if $vT_D > 2R$. For instance, if the fusion range R is set to be 10 m and the target speed v is 5 m/s (*i.e.*, 18 km/h) [14], the fusion ranges will not overlap as long as the detection period T_D is greater than 4 s.

From (11), P_{Dj} is a function of N_j . When the sensor sets $\{\mathbf{F}_j | j \geq 1\}$ are independent, $\{P_{Dj} | j \geq 1\}$ are *i.i.d.* as the numbers of sensors involved in each unit detection (*i.e.*, $\{N_j | j \geq 1\}$) are *i.i.d.* due to the Poisson process. We denote $\mathbb{E}[P_D]$ as the mean of P_{Dj} for any j , *i.e.*, $\mathbb{E}[P_D] = \mathbb{E}[P_{Dj}], \forall j$. Intuitively, the intrusion detection can be viewed as a series of infinite Bernoulli trials and the success probability of each Bernoulli trial is $\mathbb{E}[P_D]$. Accordingly, the number of unit detections before (and including) the first successful unit detection follows the geometric distribution with a mean of $1/\mathbb{E}[P_D]$. Hence the α -delay is given by the following lemma. The proof can be found in Appendix 5.

Lemma 6. *Let τ denote the α -delay of fusion-based detection. If there is no overlap between any two fusion ranges, $\tau = 1/\mathbb{E}[P_D]$, where $\mathbb{E}[P_D]$ is the average detection probability in any unit detection.*

We now discuss how to compute $\mathbb{E}[P_D]$ in Lemma 6. As P_{Dj} is a function of N_j and N_j follows the Poisson distribution, *i.e.*, $N_j \sim \text{Poi}(\rho\pi R^2)$, $\mathbb{E}[P_D]$ is given by

$$\mathbb{E}[P_D] = \sum_{N_j=0}^{\infty} P_{Dj} \cdot f_{\text{Poi}}(N_j | \rho\pi R^2), \quad (12)$$

where $f_{\text{Poi}}(k|\lambda)$ is the probability density function (PDF) of the Poisson distribution $\text{Poi}(\lambda)$. Specifically, $f_{\text{Poi}}(k|\lambda) = \lambda^k e^{-\lambda} / k!$. Note that P_{Dj} in (12) is computed using (11). Fig. 7 and Fig. 8 plot $\mathbb{E}[P_D]$ versus network density ρ and fusion range R , respectively. From Fig. 7, we can see that $\mathbb{E}[P_D]$ increases with ρ . Moreover, for a certain ρ , $\mathbb{E}[P_D]$ increases with the PSNR. From Fig. 8, we can see that $\mathbb{E}[P_D]$

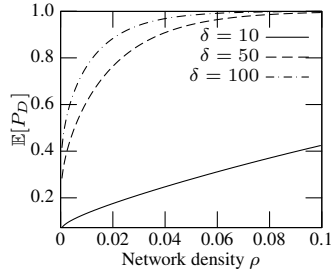


Fig. 7 Mean detection probability vs. network density ($R = 25$ m).

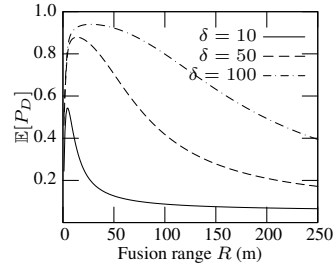


Fig. 8 Mean detection probability vs. fusion range ($\rho = 0.03$).

is a concave function of fusion range R and there exists an optimal R that maximizes $\mathbb{E}[P_D]$. When the fusion range initially increases, more sensors contribute to the data fusion resulting in better sensing quality. However, when the fusion range becomes very large, the aggregate noise starts to cancel out the benefit because the target signal decreases rapidly with the distance from the target. In other words, the measurements of sensors far away from the target contain low-quality information and hence fusing them lowers detection performance. In practice, we can choose the optimal fusion range according to numerical results.

5 Impact of Data Fusion on Spatiotemporal Coverage

In this section, we study the impact of data fusion on spatial coverage and temporal coverage in Section 5.1 and Section 5.2, respectively.

5.1 Impact of Data Fusion on Spatial Coverage

Many mission-critical applications require a high level of spatial coverage over the surveillance region. As an asymptotic case, full spatial coverage is required, *i.e.*, any target/event present in the region can be detected with a probability of at least β while the false alarm rate is below α . For random networks, a higher level of coverage always requires more sensors. Therefore, the network density for achieving full spatial coverage is an important cost metric for mission-critical applications.

Under the disc model, the sensing regions of randomly deployed sensors inevitably overlap with each other when a high level coverage is required. According to (5), we have $d\rho = \frac{1}{\pi r^2} \cdot \frac{1}{1-c} \cdot dc$. If c is close to 1, a large number of extra sensors (*i.e.*, $d\rho$) are required to eliminate a small uncovered area (*i.e.*, dc). Moreover, the situation gets worse when c increases. In this section, we are interested in how much network density can be reduced by adopting data fusion. Specifically,

we study the asymptotic relationships between the network densities for achieving full spatial coverage under the probabilistic disc and data fusion models. The results provide important insights into understanding the limitation of the disc model and the impact of data fusion on spatial coverage of random networks.

5.1.1 Full Spatial Coverage using Fixed Fusion Range

We first study the relationship between the network densities for achieving full spatial coverage under the disc and fusion models when fusion range R is a constant. We have the following theorem. The proof can be found in Appendix 6.

Theorem 1. *For uniformly deployed networks, let ρ_d and ρ_f denote the minimum network densities required to achieve the spatial coverage of c under the disc and fusion models, respectively. If the fusion range R is fixed, we have*

$$\rho_f = \mathcal{O}\left(\frac{2r^2}{R^2} \cdot \rho_d\right), \quad c \rightarrow 1^-. \quad (13)$$

Theorem 1 shows that in order to achieve full spatial coverage, ρ_f is smaller than ρ_d if $R > \sqrt{2}r$. According to (4), sensing range r is a constant independent of network density. On the other hand, fusion range R is a design parameter of the fusion model, which is mainly constrained by the communication overhead. In practice, the condition $R > \sqrt{2}r$ can be easily satisfied. For instance, the acoustic sensor on MICA2 motes has a sensing range of 3 m to 5 m if a high performance (e.g., $\alpha = 5\%$ and $\beta = 95\%$) is required [16]. On the other hand, the fusion range can be set to be much larger. For example, Fig. 6 shows that R_{opt} ranges from 5 m to 100 m when network density increases from 1.5×10^{-3} to 0.1. Therefore, according to Theorem 1, the fusion model with the optimal fusion range can significantly reduce network density for achieving a high level of coverage.

5.1.2 Full Spatial Coverage using Optimal Fusion Range

As discussed in Section 4.2.1, we can obtain the optimal fusion range via numerical experiment or analysis. Data fusion with the optimal fusion range allows the maximum number of informative sensors to contribute to the detection. The scaling law obtained with optimal fusion range will help us understand the maximum performance gain by adopting the data fusion model. The following theorem shows that ρ_f further reduces to $\mathcal{O}(\rho_d^{1-1/k})$ as long as the fusion range is optimal. The proof can be found in Appendix 7.

Theorem 2. *For uniformly deployed networks, let ρ_d and ρ_f denote the minimum network densities required to achieve the spatial coverage of c under the disc and fusion models, respectively. If the optimal fusion range R_{opt} is adopted, we have*

$$\rho_f = \mathcal{O}\left(\rho_d^{1-1/k}\right), \quad c \rightarrow 1^-. \quad (14)$$

Theorem 2 shows that if the optimal fusion range is adopted, the fusion model can significantly reduce the network density for achieving high coverage. In particular, from Theorem 2, the density ratio $\frac{\rho_f}{\rho_d} = \mathcal{O}(\rho_d^{-1/k}) = 0$ when $c \rightarrow 1^-$, which means ρ_f is insignificant compared with ρ_d for achieving high coverage. Theorem 2 is applicable to the scenarios where the physical signal follows the power law decay with path loss exponent k , which are widely assumed and verified in practice. We note that the path loss exponent k typically ranges from 2.0 to 5.0 [25, 19]. In particular, the propagation of acoustic signals in free space follows the inverse-square law, *i.e.*, $k = 2$, and therefore $\rho_f = \mathcal{O}(\sqrt{\rho_d})$.

5.1.3 Impact of Signal-to-Noise Ratio

In this section, we study the impact of PSNR on the results derived in the previous sections. PSNR is an important system parameter which is determined by the property of target, noise level, and sensitivity of sensors. We have the following theorem.

Theorem 3. *For uniformly deployed networks, if the fusion range R is fixed, we have*

$$\frac{\rho_f}{\rho_d} = \mathcal{O}(\delta^{2/k}), \quad c \rightarrow 1^-. \quad (15)$$

Proof. As $w(x) = \Theta(x^{-k})$, $w^{-1}(x) = \Theta(x^{-1/k})$. According to (4), the sensing range $r = \Theta(\delta^{1/k})$. As $\lim_{c \rightarrow 1^-} \frac{\rho_f}{\rho_d} \leq \frac{2r^2}{R^2} = \Theta(\delta^{2/k})$, we have (15). \square

Theorem 3 suggests that for a fixed R , the relative cost between the fusion and disc models is affected by the PSNR δ . Specifically, the fusion model requires fewer sensors to achieve full spatial coverage than the disc model if the PSNR is low. On the other hand, the disc model suffices only if the PSNR is *sufficiently* high. Intuitively, sensor collaboration is more advantageous when the PSNR is low to moderate. However, when the PSNR is *sufficiently* high, the detection performance of a single sensor is satisfactory and the collaboration among multiple sensors may be unnecessary.

5.2 Impact of Data Fusion on Temporal Coverage

Many mission-critical real-time applications require detection delay to be as small as possible [20, 45]. As an asymptotic case, the α -delay approaches one, *i.e.*, any target can be detected almost surely in the first detection period after its appearance, which is referred to as the *instant detection*. As a smaller detection delay always requires more sensors, the network density for achieving instant detection is an important cost metric for mission-critical real-time sensor networks. In this section,

we investigate the required network density for achieving instant detection under both the disc and fusion models. According to Lemma 2 and 6, the network density under both models approaches infinity² when the α -delay reduces to one. However, the speed that the network density increases is different. In this section, we study the ratio of network densities for instant detection under the two models, which characterize the relative cost of the two models when detection delay is minimized. The result provides important insights into understanding the limitation of the disc model and the impact of data fusion on the performance of real-time WSNs for intrusion detection. In the rest of this section, we first discuss the case that the target discs and fusion ranges under the disc and fusion models do not overlap in Section 5.2.1, and then generalize the results in Section 5.2.2.

5.2.1 Network Density for Achieving Instant Detection

We have the following lemma. The proof can be found in Appendix 8.

Lemma 7. *Let ρ_f and ρ_d denote the network densities for achieving α -delay of τ under the fusion and disc models, respectively. If there is no overlap between target discs and fusion ranges under the two models, respectively, there exists $\xi \in (0, 1)$ such that*

$$\frac{2}{\gamma^2 R^2} \cdot r^2 \leq \lim_{\tau \rightarrow 1^+} \frac{\rho_f}{\rho_d} \leq \frac{2}{\xi \gamma^2 R^2} \cdot r^2, \quad (16)$$

where $\gamma = -\frac{\mu_s}{\sqrt{\sigma_s^2 + \sigma^2}}$.

Note that ξ is a function of γ (given by (30)). According to Lemma 7, $\lim_{\tau \rightarrow 1^+} \rho_f / \rho_d$ is largely affected by the sensing range of a single sensor. According to (4), the sensing range r is determined by the requirements on false alarm rate and detection probability (i.e., α and β), as well as the PSNR δ . Moreover, as discussed in Section 4.1.3, β is a constant close to one. Accordingly, we only analyze the impacts of α and δ on the network density for achieving instant detection. We have the following theorem. The proof can be found in Appendix 9.

Theorem 4. *If there is no overlap between target discs and fusion ranges under the disc and fusion models, respectively, for given path loss exponent k , the ratio of network densities for instant detection under the two models has an asymptotic tight bound of*

$$\frac{\rho_f}{\rho_d} = \Theta \left(\left(\frac{\delta}{Q^{-1}(\alpha)} \right)^{2/k} \right), \quad \tau \rightarrow 1^+. \quad (17)$$

Theorem 4 suggests that, for a certain path loss exponent k , the relative cost for instant detection between the fusion and disc models depends on the required

² Numerically, the network density ρ will not be very large when the α -delay approaches one. For instance, according to Lemma 2, suppose the sensing range r is 5 m, the α -delay under the disc model is $1 + 10^{-5}$ when $\rho = 0.15$.

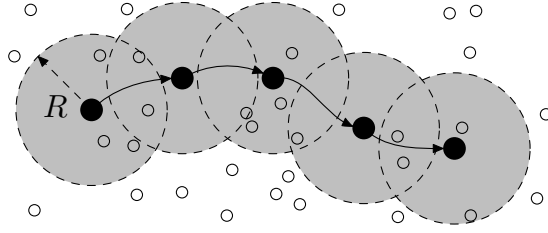


Fig. 9 The overlap case under the data fusion model. The void circles represent sensors; the solid circles represent the target in different sampling intervals; the dashed discs represent the fusion ranges.

false alarm rate α and PSNR δ . First, when $\alpha \rightarrow 0$, $Q^{-1}(\alpha) \rightarrow \infty$ and hence $\lim_{\tau \rightarrow 1^+} \rho_f / \rho_d \rightarrow 0$. It suggests that data fusion can significantly reduce network density when a small false alarm rate is required. Second, $\lim_{\tau \rightarrow 1^+} \rho_f / \rho_d$ increases with δ , which suggests that the advantage of data fusion diminishes as the PSNR increases. Moreover, the path loss exponent k determines the order of density ratio with regard to the PSNR. Intuitively, sensor collaboration is more advantageous when the PSNR is low. However, when the PSNR is *sufficiently* high, the detection performance of a single sensor is satisfactory and the collaboration among multiple sensors may be unnecessary.

5.2.2 Extension to General Target Speed and Detection Period

In previous sections, we assume that there is no overlap between any two target discs and fusion ranges under the disc and fusion models, respectively. However, fusion ranges may overlap if the target speed is low or the detection period T_D is short, as illustrated in Fig. 9. In this section, we will generalize the previous analyses without the no-overlap limitation. When there is no overlap, the unit detections are independent from each other. As a result, the index of first successful unit detection (*i.e.*, J) follows the geometric distribution and the α -delay can be computed as the mean of the geometric distribution. In contrast, when target discs or fusion ranges can overlap, the detection results in different unit detections are statistically *correlated* due to the possible common sensors shared by different unit detections. Hence, J does not follow the geometric distribution anymore. Therefore, the correlation among unit detections substantially complicates the analysis of α -delay. As a result, it is difficult to obtain the closed-form formula of α -delay. Instead, we aim to find the bound of α -delay in this section. The lower bound of α -delay under the disc model is given by the following lemma. The proof can be found in Appendix 10.

Lemma 8. *Let τ denote the α -delay under the probabilistic disc model. We have*

$$\tau \geq \frac{1}{1 - e^{-\rho\pi r^2}}.$$

Compared with the results in Lemmas 2 and 8, we can see that the α -delay is minimized for the no-overlap case. Intuitively, the area covered by the union of target discs is maximized in the no-overlap case, which yields the maximum overall detection probability for a given number of detection periods and in turn leads to the minimum detection delay.

The upper bound of α -delay under the data fusion model is given by the following lemma. The proof can be found in Appendix 11.

Lemma 9. *Let τ denote the α -delay of fusion-based detection. We have $\tau \leq \mathbb{E}[1/P_D]$, where P_D is the detection probability in any unit detection.*

As $1/P_D$ is a convex function of P_D , according to Jensen's inequality, $\mathbb{E}[1/P_D] \geq 1/\mathbb{E}[P_D]$, where $1/\mathbb{E}[P_D]$ is the α -delay when there is no overlap between any two fusion ranges. We now discuss how to compute $\mathbb{E}[1/P_D]$ in Lemma 9. As P_{D_j} is a function of N_j which follows the Poisson distribution, i.e., $N_j \sim \text{Poi}(\rho\pi R^2)$, $\mathbb{E}[1/P_D]$ can be numerically computed by averaging $\frac{1}{P_{D_j}}$ over the distribution of N_j .

With the lower and upper bounds of α -delay under the disc and fusion models, respectively, we can derive the asymptotic bound of ratio of network densities required by the two models to achieve instant detection. As it is more challenging to handle the expression $\mathbb{E}[1/P_D]$ in Lemma 9 than $\mathbb{E}[P_D]$ in Lemma 6, we will employ substantially different technique to analyze the density ratio. We have the following theorem. The proof can be found in Appendix 12.

Theorem 5. *Let ρ_f and ρ_d denote the network densities for achieving α -delay of τ under the value fusion and disc models, respectively. For given path loss exponent k , the ratio of network densities for instant detection has an asymptotic upper bound of*

$$\lim_{\tau \rightarrow 1^+} \frac{\rho_f}{\rho_d} = \mathcal{O} \left(\left(\frac{\delta}{Q^{-1}(\alpha)} \right)^{2/k} \right). \quad (18)$$

Different from the result in Theorem 4 which is the asymptotic *tight* bound of the density ratio, Theorem 5 gives the asymptotic *upper* bound. In Section 7.2.3, we will compare the density ratios under the overlap and no-overlap cases through simulations. Moreover, as target speed is an important factor of the overlap/no-overlap condition, we also evaluate the impact of target speed on the density ratio.

6 Implications of Results and Discussions

In this section, we first summarize the implications of the theoretical results derived in previous sections, which provide important insights into understanding the applicability of the disc model and the data fusion model in various application scenarios. We then discuss several issues that have not been addressed.

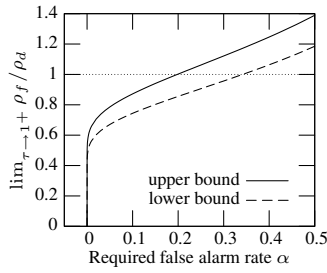


Fig. 10 Density ratio vs. required false alarm rate ($k = 2$, $\delta = 50$, $R = 37$ m).

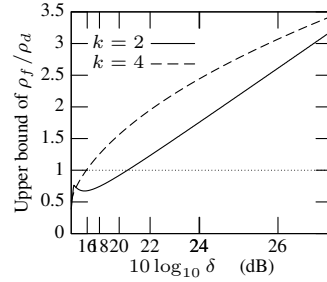


Fig. 11 Upper bound of density ratio vs. SNR ($\alpha = 0.1\%$).

6.1 Implications of Results

6.1.1 Data Fusion Reduces Network Density

According to Theorem 2, when the coverage of random networks approaches one, ρ_d increases significantly faster than ρ_f , especially for a small path loss exponent. For instance, when $k = 2$ (which typically holds for acoustic signals), $\rho_f = \mathcal{O}(\sqrt{\rho_d})$. This result implies that the existing analytical results based on the disc model (e.g., [23, 46, 52, 29, 4]) significantly overestimate the network density required for achieving full spatial coverage of random networks. Data fusion can reduce network density for achieving instant detection as well. According to Theorem 4, when the detection delay is minimized (i.e., $\tau \rightarrow 1^+$), $\rho_f / \rho_d \rightarrow 0$ when $\alpha \rightarrow 0$. Therefore, if a small α is required, $\rho_f < \rho_d$ for instant detection, i.e., the fusion model requires lower network density than the disc model. In other words, data fusion is effective in reducing detection delay and false alarms. For instance, Fig. 10 plots the lower and upper bounds of the density ratio when the α -delay is minimized, which is given by Lemma 7. We set the PSNR δ to be 50 (i.e., 17 dB) according to the measurements in the vehicle detection experiments based on MICA2 [16] and ExScal [17] motes. The fusion range R is optimized to be 37 m. From the figure, we can see that if $\alpha < 0.2$, the fusion model outperforms the disc model. In practice, most mission-critical surveillance systems require a small α . For example, in the vehicle detection system [20] and the acoustic shooter localization system [45], the false alarm rates are tuned to be near zero. Therefore, data fusion can significantly reduce the network density for these mission-critical surveillance systems.

6.1.2 Disc Model Suffices for High-SNR Detection

On the other hand, Theorem 3 shows that the disc model may lead to similar or even lower network density than the fusion model for achieving full spatial coverage if PSNR is sufficiently high. Similarly, according to Theorem 4, $\lim_{\tau \rightarrow 1^+} \rho_f / \rho_d$ increases with δ for fixed α . Therefore, if the PSNR is high enough such that

$\lim_{\tau \rightarrow 1^+} \rho_f / \rho_d > 1$, the disc model is superior to the fusion model in achieving instant detection. For instance, Fig. 11 plots the upper bound of density ratio versus SNR under various path loss exponents when α -delay is minimized, which is given by Lemma 7. From the figure, we can see linear and concave relationships between the density ratio and PSNR when k is 2.0 and 4.0, respectively, which are consistent with Lemma 6. Moreover, if the PSNR is sufficiently high (*e.g.*, 22 dB), the disc model outperforms the fusion model. However, the noise experienced by a sensor comes from various sources, *e.g.*, the random disturbances in the environment and the electronic noise in the sensor's circuit. Thus, the PSNR depends on the characteristics of targets, the environment, and the sensor device. In the vehicle detection experiments based on low-power motes, *e.g.*, MICA2 [16] and ExScal [17], the PSNRs are usually low to moderate (≤ 17 dB). In such a case, data fusion can effectively reduce the network density required to achieve a high level of coverage or a short detection delay.

6.1.3 Design of Data Fusion Algorithms

Our results provide several important guidelines on the design of data fusion algorithms for large-scale WSNs. First, data fusion is very effective in reducing network density for achieving a high level of coverage or a short detection delay. In particular, Theorems 3-5 suggest that the performance gain of data fusion increases when the PSNR is lower. Therefore, data fusion should be employed for low-SNR deployments when a high level of coverage or a short detection delay is required. Second, Theorems 1, 2 and Lemma 7 suggest that fusion range plays an important role in the achievable performance of data fusion. Particularly, as discussed in Section 4.2.1, the optimal fusion range that maximizes the spatial coverage of random networks increases with network density and can be numerically computed. However, a larger fusion range may lead to longer transmission distances and more sensors that take part in data fusion. Investigating the optimal fusion range under joint constraints of coverage, detection delay and communication is left for the future work.

6.2 Discussions

We now discuss several issues that have not been addressed.

6.2.1 Noise Models

In the proofs of Lemma 3, 4 and 5 the fusion statistic Y has a component $\sum_{i \in \mathcal{F}(p)} n_i$. According to the CLT, this component approximately follows the normal distribution if $\{n_i\}$ are *i.i.d.*. Therefore, the assumption of *i.i.d.* Gaussian noises made in Section 3.1.1 can be relaxed to *i.i.d.* noises that follow any distribution, when the

number of sensors taking part in data fusion is large enough. In practice, the accuracy of this approximation is satisfactory when $N(p) \geq 20$ [33]. In particular, the distribution of noise will not affect the asymptotic scaling laws in Sections 5.1 and 5.2, as $N(p)$ is large in the asymptotic scenarios where $c \rightarrow 1^-$.

6.2.2 Signal Decay Laws

The main objective of this chapter is to explore the fundamental limits of coverage and detection delay based on data fusion model in target surveillance applications, in which sensors measure the signals emitted by the target. The proofs of all lemmas and Theorem 1 are not dependent on the form of the signal decay function $w(\cdot)$. Therefore, these results hold under *arbitrary* bounded decreasing function $w(\cdot)$. However, Theorems 2-5 are only applicable for the applications where the target signal follows the power law decay, *i.e.*, $w(x) = \Theta(x^{-k})$. We acknowledge that most mechanical and electromagnetic waves follow the power law decay in propagation. In particular, in open space, inverse-square law (*i.e.*, $k = 2$) [11] applies to various physical signals such as sound, light and radiation. We note that if a sensor is lifted above the ground, its received signal energy can be affected by the height. However, as Theorems 2-5 only depend the asymptotic power law decay, they still hold if the height only introduces constant gain coefficient to the decay model. In the future work, we will investigate if the height can lead to an asymptotic decay model that is different from the power law decay. Moreover, we will extend our analyses to address other decay laws such as exponential decay in diffusion processes [40].

6.2.3 Data Fusion Models

Theorems 1, 2, 3 and 5 give the upper bounds of network density under the fusion model presented in Section 3.1.3. If more efficient fusion models are employed, the coverage performance as well as detection delay will be further improved. Therefore, more efficient fusion model can reduce the network density for achieving a certain level of coverage or detection delay. As a result, the upper bounds of network density derived in this chapter still hold. Exploring the impact of efficiency of fusion models on network density is left for future work.

7 Evaluation

In this section, we conduct extensive simulations based on real data traces as well as synthetic data to evaluate the spatiotemporal coverage in non-asymptotic and asymptotic cases, respectively.

7.1 Trace-driven Simulations

7.1.1 Methodology and Settings

We first conduct simulations using the data traces collected in the DARPA SensIT vehicle detection experiment [14]. In the experiments, 75 WINS NG 2.0 nodes are deployed to detect amphibious assault vehicles (AAVs) driving through the surveillance region. We refer to [14] for detailed setup of the experiments. The dataset used in our simulations includes the ground truth data and the acoustic time series recorded by 20 nodes at a frequency of 4960 Hz when a vehicle drives through. The ground truth data include the positions of sensors and the trajectory of the AAV recorded by a global positioning system (GPS) device.

Sensors' sensing ranges under the probabilistic disc model are determined individually to meet the detection performance requirements ($\alpha = 5\%$, $\beta = 95\%$). The resulted sensing ranges are from 22.5 m to 59.2 m with the average of 43.2 m. Such a significant variation is due to several issues including poor calibration and complex terrain. In our simulation, we deploy random or regular networks with size of $1000 \times 1000 \text{ m}^2$. Each sensor in the simulation is associated with a real sensor chosen at random. For each deployment, we evaluate the spatial coverage and α -delay under both the disc and fusion models, respectively.

For evaluating spatial coverage, we divide the region into 1000×1000 grids. Under the disc model, the coverage is estimated as the ratio of grid points that are covered by discs. Under the fusion model, the coverage is estimated as the ratio of (α, β) -covered grid points. Specifically, for a target that appears at a grid point, each sensor makes a measurement which is set to be the signal energy gathered by the associated real sensor at a similar distance to vehicle in the data trace. A cluster is formed around the sensor with the highest reading, which fuses sensor measurements for detection.

For evaluating α -delay, the target initially appears at the origin, and moves along the X -axis at a speed of 10 m/s. The detection period T_D is set to be 60 s. Under the disc model, once the target enters the sensing range of a sensor, the sensor makes a detection decision by comparing its measurement against the detection threshold t derived in Section 4.1.1. Under the fusion model, sensors fuse their measurements to detect the target as discussed in Section 3.1.3. The α -delay is computed as the average number of detection periods before the target is first detected in each run.

7.1.2 Simulation Results

Fig. 12 plots the the numbers of uniformly deployed sensors under the disc and fusion models as well as the corresponding density ratio versus the achieved spatial coverage. We can see that the disc model suffices if a moderate level of coverage is required. However, the fusion model is more effective for achieving high coverage. In particular, the fusion model with a fusion range of 200 m saves more than 50% sensors when the coverage is greater than 0.75. We note that the average number

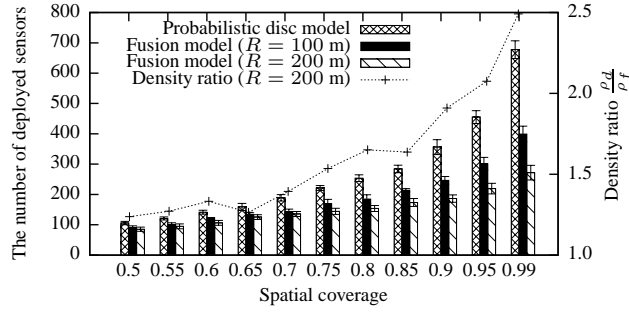


Fig. 12 The number of deployed sensors in random networks vs. achieved spatial coverage.

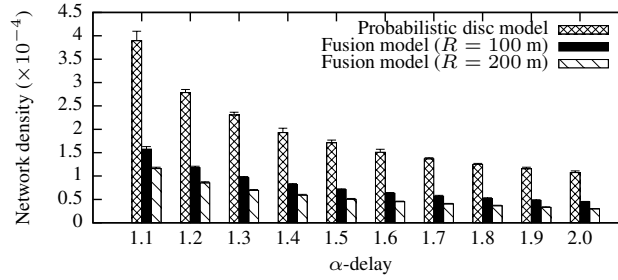


Fig. 13 The network density vs. achieved α -delay.

of sensors taking part in data fusion is within 30 and hence will not introduce high communication overhead. According to Theorem 1, the limit of $\frac{\rho_d}{\rho_f}$ is $\frac{R^2}{2r^2}$ when the coverage approaches one. We will evaluate the coverage performance in asymptotic case through simulations based on synthetic data in Section 7.2. Fig. 13 plots the network density versus the achieved α -delay under various settings. We can see that the fusion model is more effective than the disc model for achieving short α -delay. In particular, the fusion model with a fusion range of 100 m saves more than 50% sensors when the α -delay is less than 2. We note that the average number of sensors taking part in data fusion is within 20 and hence will not introduce high communication overhead.

7.2 Simulations Based on Synthetic Data

7.2.1 Numerical Settings

In addition to trace-driven simulations, we also conduct extensive simulations based on synthetic data. These simulations allow us to evaluate the theoretical results in a wide range of settings. We adopt the signal decay function in (1) with $k = 2$. Both the mean and variance of the Gaussian noise generator, μ and σ^2 , are set to be 1. We

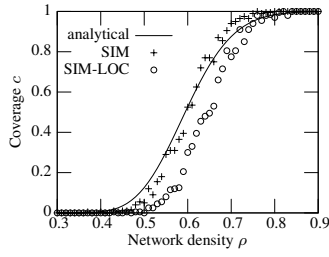


Fig. 14 Spatial coverage of random networks vs. network density ($\delta = 4$, $R = 5$ m).

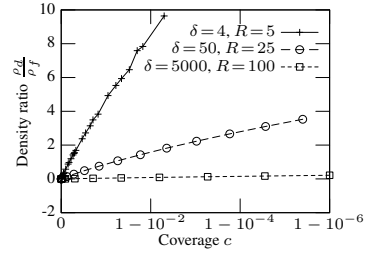


Fig. 15 Density ratio $\frac{\rho_d}{\rho_f}$ of random networks vs. spatial coverage in \log_{10} scale with various PSNRs.

set the target's source energy, *i.e.*, S_0 , to be 4, 50, and 5000, so that the SNRs in the simulations are consistent with several real experiments [9, 16, 17, 14].

For evaluating coverage, as proved in Lemma 3, it suffices to measure the probability that a point is covered for evaluating the coverage of a random network. Hence, we let the target appear at a fixed point p and deploy random networks with size of $4R \times 4R$ centered at p . For each deployment, $P_D(p)$ is estimated as the fraction of successful detections. The spatial coverage is estimated as the fraction of deployments whose $P_D(p)$ is greater than β . We also evaluate the impact of localization error by integrating a simple localization algorithm. Specifically, for each detection, if a sensor's reading exceeds $S_0 \cdot w(R) + \mu$, it will take part in the target localization. The target is localized as the geometric center of the sensors participating in the localization. For a regular network, it suffices to measure the fraction of covered area in a grid for evaluating the coverage of the whole network. In our simulations, we find the minimum network density with which 10×10 points in the grid are covered.

For evaluating detection delay, the target initially appears at the origin, and moves along the X -axis at a speed of $2R$ per detection period. We evaluate the impact of constant target localization error as follows. Suppose the real target position is at $P(x, y)$ when sensors take measurements, while the target position localized by the network is at $P'(x + \epsilon \cos \theta, y + \epsilon \sin \theta)$, where ϵ is a specified constant and θ is picked uniformly from $[0, 2\pi)$. Sensors within the fusion range centered at P' fuse their measurements and make the detection decision. We also evaluate the impact of the overlap/no-overlap condition by comparing the simulation results under the overlap and no-overlap cases. For the overlap case, the target moves $\frac{R}{2}$ and $\frac{r}{2}$ in each detection period under the fusion and disc models, respectively; for the no-overlap case, it moves $2R$ and $2r$, respectively.

7.2.2 Spatial Coverage

We first present the simulation results if sensors are randomly deployed. The first set of simulations evaluate the accuracy of the approximate formula given in Lemma 4.

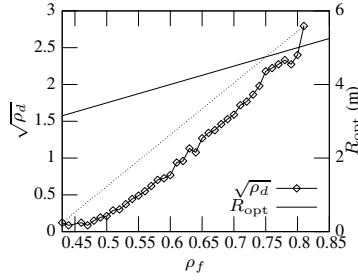


Fig. 16 $\sqrt{\rho_d}$ vs. ρ_f of random networks with optimal fusion range R_{opt} ($\delta = 4$).

Fig. 14 plots the analytical and measured coverage versus network density. The curves labelled with SIM-LOC and SIM represent the measured results with and without accounting for localization error, respectively. We can see that the simulation result matches well the analytical result given by (7). A network density of 0.8 is enough to provide high coverage under the fusion model, where the SNR is very low ($\delta = 4$). When there is localization error, a maximum deviation of about 0.2 from the analytical result can be seen from Fig. 14. The coverage decreases in the presence of localization error as sensors received weaker signals when the target cannot be accurately localized. However, the impact of localization error diminishes when $c \rightarrow 1^-$.

The second set of simulations evaluate the impact of SNR on the asymptotic network densities. Fig. 15 plots the network density ratio $\frac{\rho_d}{\rho_f}$ versus the achieved coverage under various PSNRs, where ρ_d is computed by (5) and ρ_f is obtained in simulations, respectively. The x -axis is plotted in \log_{10} scale. We can see that the density ratio increases with the coverage, *i.e.*, the fusion model becomes more effective for achieving higher coverage. Moreover, the density ratio decreases with the PSNR, which conforms to the result of Theorem 3. For instance, to achieve a high coverage of 0.99, the density ratio $\frac{\rho_d}{\rho_f}$ is about 8 when $\delta = 4$. The density ratio decreases to about 2 when $\delta = 50$. This result shows that data fusion is effective in the scenarios with low SNRs. When $\delta = 5000$, the disc model suffices. These results are consistent with the analysis in Section 5.1.3.

The third set of simulations evaluate the asymptotic relationship between ρ_d and ρ_f when the fusion range is optimized. In Fig. 16, the X - and Y -axis of each data point represent the required network densities for achieving the same coverage that approaches to one under the disc and fusion models, respectively. Note that the Y -axis is plotted in square root scale. The optimal fusion range R_{opt} plotted in Fig. 16 is computed for each given ρ_f by numerically maximizing (7). We can see from Fig. 16 that the relationship between $\sqrt{\rho_d}$ and ρ_f is convex and therefore conforms to the theoretical result $\rho_f = \mathcal{O}(\sqrt{\rho_d})$ according to Theorem 2. Moreover, R_{opt} increases with ρ_f , which is also consistent with the analysis in Section 4.2.1.

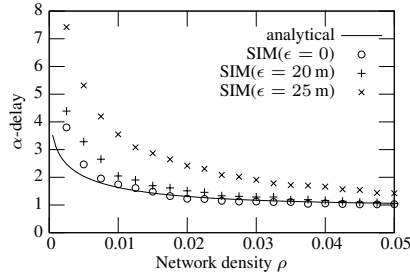


Fig. 17 α -delay vs. network density under data fusion model.

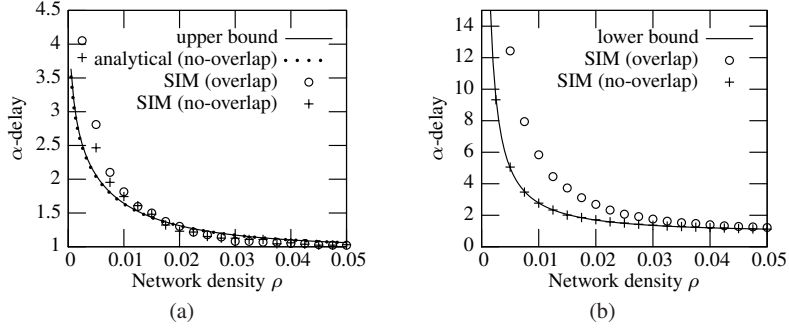


Fig. 18 α -delay vs. network density. (a) Data fusion model. (b) Disc model.

7.2.3 Temporal Coverage

We first evaluate the analytical result on the α -delay of fusion-based detection. Fig. 17 plots the α -delay versus the network density. The curve labeled with “analytical” plots the α -delay computed according to Lemma 6 and Eq. (12). The data points labeled with “SIM(ϵ)” represent the simulation results with a constant localization error ϵ . From the figure, we can see that the α -delay decreases with the network density. The simulation result without localization error (*i.e.*, $\epsilon = 0$) confirms the analytical result when the network density is greater than 0.01. When ρ is smaller than 0.01, the simulation result starts to deviate from the analytical result. This is due to the approximation made in the derivation of P_D in Section 4.2.2. However, we can see that the maximum error between the analytical and simulation results falls within one detection period. Fig. 17 also shows that the impact of localization error is small. The simulation result has a considerable deviation from the analytical result only when the localization error is equal to the fusion range (25 m). In such a case, the target falls completely outside of the fusion range. Moreover, the impact of localization error diminishes as the network density increases. This result demonstrates the robustness of our analysis with respect to localization error, especially in achieving instant detection.

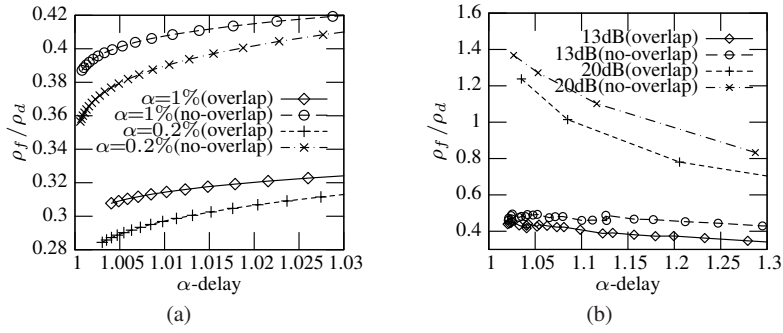


Fig. 19 Density ratio vs. α -delay. (a) Given different α (SNR = 10 dB). (b) Given different SNRs ($\alpha = 1\%$).

The second set of simulations evaluate the impact of overlap/no-overlap condition on the α -delay under the disc and fusion models, respectively. Fig. 18(a) plots the α -delay versus the network density under the value fusion model. The curves labeled with “analytical (no-overlap)” and “upper bound” plot the α -delay under the no-overlap case (given by Lemma 6) and its upper bound (given by Lemma 9), respectively. We can see that the two analytical results are very close. The other two curves plot the simulation results for the overlap and no-overlap cases, respectively. The simulation results closely match the analytical results when the network density is greater than 0.02. When ρ is smaller than 0.01, the deviation between the analytical and simulation results is due to the approximation made in the derivation of P_D . Moreover, we can see from Fig. 18(a) that the overlap/no-overlap condition has little impact on the α -delay under the fusion model. Fig. 18(b) plots the α -delay under the disc model. Note that the lower bound given by Lemma 8 is also the analytical result of α -delay under the no-overlap case given by Lemma 2. We can see that the simulation results confirm the analytical results under the disc model. Moreover, the α -delay significantly increases under the overlap case. Hence, the overlap/no-overlap condition has significant impact on the α -delay under the disc model.

We now evaluate the impact of false alarm rate and SNR on the density ratio. Fig. 19(a) plots the ratio of network densities required by the data fusion and disc models to achieve the same α -delay given various false alarm rates. We can see from Fig. 19(a) that the disc model requires more than twice sensors when the α -delay approaches to one. Both for the value and decision fusion models, the density ratio decreases if a lower α is required, which is consistent with Theorems 4 and 5. Moreover, from the two figures, we can see that the density ratio under the overlap case is smaller than that under the no-overlap case. This is consistent with our observation in the previous set of simulations, *i.e.*, the overlap condition has little impact on the fusion model while leads to significant increase of α -delay under the disc model. Fig. 19(b) plots the ratio of network densities required by the data fusion and disc models given various SNRs. From Fig. 19(b), we can see that the density

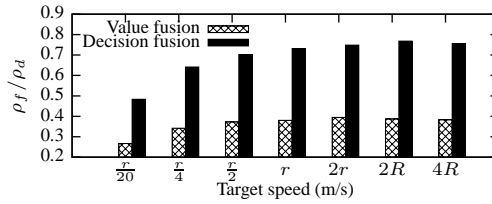


Fig. 20 Density ratio vs. target speed (SNR = 13 dB, $\alpha = 5\%$, $\tau = 1.05$, $r = 2.25$ m, $R = 8$ m, $T = 1$ s).

ratio increases with SNR, which is consistent Theorems 4 and 5. For instance, if the SNR is 13 dB, the density ratio ρ_f/ρ_d is about 0.5 when the α -delay reduces to one. However, if the SNR increases to 20 dB, ρ_f/ρ_d is greater than 1.2 and hence the disc model requires fewer sensors than the fusion model.

As target speed is an important factor of the overlap/no-overlap condition, we finally evaluate its impact on the density ratio. Fig. 20 shows the density ratio versus the target speed. We can see that the density ratio significantly increases when the target speed increases from $\frac{r}{20}$ to $2r$. This is due to the significant impact of overlap condition on the disc model, as observed in Fig. 18(b). Hence, the data fusion models are more robust than the disc model in detecting slowly moving targets.

8 Conclusion

Spatiotemporal coverage is an important performance requirement of many critical sensor network applications. In this paper, we explore the fundamental limits of spatiotemporal coverage based on stochastic data fusion models that jointly process noisy measurements of sensors. The scaling laws between spatiotemporal coverage, network density, and SNR are derived. Data fusion is shown to significantly improve spatiotemporal coverage by exploiting the collaboration among sensors. Our results help understand the limitations of the existing analytical results based on the disc model and provide key insights into the design and analysis of WSNs that adopt data fusion algorithms. Our analyses are verified through simulations based on both synthetic data sets and data traces collected in a real deployment for vehicle detection.

Appendix 1: Proof of Lemma 2

Proof. As shown in [29], when the sensors are deployed according to the Poisson process, the probability that there is at least one sensor in a target disc is $p = 1 - e^{-\rho\pi r^2}$. Suppose the target is detected in the J th ($J \geq 1$) detection period. As there is no overlap between any two target discs, the unit detections are

independent from each other. Therefore, J follows the geometric distribution with a success probability of p in each Bernoulli trial (*i.e.*, each unit detection). Moreover, according to the definition of r in (4), the false alarm rate in each unit detection is no greater than α . According to Definition 3, the α -delay is given by $\tau = \mathbb{E}[J] = \frac{1}{p} = \frac{1}{1 - e^{-\rho\pi r^2}}$.

Appendix2: Proof of Lemma 3

Proof. We first discuss the necessary and sufficient condition that p is (α, β) -covered. When no target is present, all sensors measure *i.i.d.* noises and hence $Y|H_0 = \sum_{i \in \mathbf{F}(p)} n_i \sim \mathcal{N}(\mu N(p), \sigma^2 N(p))$. Therefore, the false alarm rate is $P_F = \mathbb{P}(Y \geq T|H_0) = Q\left(\frac{T - \mu N(p)}{\sigma \sqrt{N(p)}}\right)$, where T is the detection threshold. As P_D is a non-decreasing function of P_F [44], it is maximized when P_F is set to be the upper bound α . Such a scheme is referred to as the constant false alarm rate detector [44]. Let $P_F = \alpha$, the optimal detection threshold can be derived as $T_{\text{opt}} = \mu N(p) + \sigma Q^{-1}(\alpha) \sqrt{N(p)}$.

When the target is present, we have

$$Y|H_1 = \sum_{i \in \mathbf{F}(p)} s_i + n_i \sim \mathcal{N}(\mu N(p) + \sum_{i \in \mathbf{F}(p)} s_i, \sigma^2 N(p)).$$

Therefore, the detection probability at p is given by

$$P_D(p) = \mathbb{P}(Y \geq T|H_1) = Q\left(\frac{T - \mu N(p) - \sum_{i \in \mathbf{F}(p)} s_i}{\sigma \sqrt{N(p)}}\right).$$

By replacing T with T_{opt} and solving $P_D(p) \geq \beta$, we have the necessary and sufficient condition that p is (α, β) -covered:

$$\frac{\sum_{i \in \mathbf{F}(p)} s_i}{\sqrt{N(p)}} \geq \sigma (Q^{-1}(\alpha) - Q^{-1}(\beta)). \quad (19)$$

As the random network is stationary, the fraction of covered area equals the probability that an arbitrary point is covered by the network [29]. Therefore, the spatial coverage of the network is given by (6). \square

Appendix 3: Proof of Lemma 4

Proof. We first prove that the $\{s_i | i \in \mathbf{F}(p)\}$ are *i.i.d.* for given p and derive the formulas for μ_s and σ_s^2 . As sensors are deployed uniformly and independently,

$\{d_i|i \in \mathbf{F}(p)\}$ are *i.i.d.* for given p , where d_i is the distance between sensor i and point p . To simplify our discussion, we now temporarily assume that there is no localization error, *i.e.*, $\epsilon = 0$. Therefore, $\{s_i|i \in \mathbf{F}(p)\}$ are *i.i.d.* for given p , as s_i is a function of d_i . Suppose the coordinates of point p and sensor i are (x_p, y_p) and (x_i, y_i) , respectively. The posterior PDF of (x_i, y_i) is $f(x_i, y_i) = \frac{1}{\pi R^2}$ where $(x_i - x_p)^2 + (y_i - y_p)^2 \leq R^2$. Hence, the posterior CDF of d_i is given by $F(d_i) = \int_0^{2\pi} d\theta \int_0^{d_i} \frac{1}{\pi R^2} \cdot x dx = \frac{d_i^2}{R^2}$ where $d_i \in [0, R]$. Therefore, we have

$$\mu_s = \int_0^R s_i dF(d_i) = \frac{2S_0}{R^2} \cdot \int_0^R xw(x)dx, \quad (20)$$

$$\sigma_s^2 = \int_0^R s_i^2 dF(d_i) - \mu_s^2 = \frac{2S_0^2}{R^2} \int_0^R xw^2(x)dx - \mu_s^2. \quad (21)$$

By letting $\mu_0 = \frac{2}{R^2} \int_0^R xw(x)dx$ and $\sigma_0^2 = \frac{2}{R^2} \int_0^R xw^2(x)dx - \mu_0^2$, we have $\mu_s = S_0\mu_0$ and $\sigma_s^2 = S_0^2\sigma_0^2$.

A straightforward approximation is to replace $\sum_{i \in \mathbf{F}(p)} s_i$ in (6) with its mean $\mu_s N(p)$. However, doing so ignores the distribution of $\sum_{i \in \mathbf{F}(p)} s_i$. As $N(p)$ follows the Poisson distribution, $\sum_{i \in \mathbf{F}(p)} s_i$ follows the *compound Poisson distribution*, which has no closed-form PDF and CDF. We approximate the compound Poisson distribution using the normal distribution. The intuition behind this approximation is the CLT by assuming $N(p)$ is a constant. Therefore, $\sum_{i \in \mathbf{F}(p)} s_i \sim \mathcal{N}(\mu_s N(p), \sigma_s^2 N(p))$. When the target is present, $Y|H_1 = \sum_{i \in \mathbf{F}(p)} s_i + \sum_{i \in \mathbf{F}(p)} n_i$. As the sum of two independent Gaussians is also Gaussian, $Y|H_1$ follows the normal distribution, *i.e.*, $Y|H_1 \sim \mathcal{N}(\mu_s N(p) + \mu N(p), \sigma_s^2 N(p) + \sigma^2 N(p))$. Therefore, the detection probability at point p is given by $P_D(p) = \mathbb{P}(Y \geq T|H_1) \simeq Q\left(\frac{T - \mu_s N(p) - \mu N(p)}{\sqrt{\sigma_s^2 + \sigma^2} \cdot \sqrt{N(p)}}\right)$. By replacing T with the optimal detection threshold T_{opt} (derived in the proof of Lemma 3) and solving $P_D(p) \geq \beta$, the condition that p is (α, β) -covered is given by $N(p) \geq \gamma(R)$. The approximate formula of spatial coverage is then given by

$$c \simeq \mathbb{P}(N(p) \geq \gamma(R)) = 1 - F_{\text{Poi}}(\gamma(R)|\rho\pi R^2), \quad (22)$$

where $F_{\text{Poi}}(\cdot|\lambda)$ is the CDF of the Poisson distribution $\text{Poi}(\lambda)$. When $\rho\pi R^2$ is large enough, the Poisson distribution $\text{Poi}(\rho\pi R^2)$ can be excellently approximated by the normal distribution $\mathcal{N}(\rho\pi R^2, \rho\pi R^2)$. Therefore, Eq. (22) can be further approximated by (7). \square

Appendix 4: Proof of Lemma 5

Proof. For any point p , $\sum_{i \in \mathbf{F}(p)} s_i \geq S_0 \cdot w(R+\epsilon) \cdot N(p)$, as $s_i \geq S_0 \cdot w(R+\epsilon)$ for any sensor i in $\mathbf{F}(p)$. If $\frac{S_0 \cdot w(R+\epsilon) \cdot N(p)}{\sqrt{N(p)}} \geq \sigma (Q^{-1}(\alpha) - Q^{-1}(\beta))$, Eq. (19) must hold. Therefore, by solving $N(p)$, the sufficient condition that p is (α, β) -covered is $N(p) \geq \Gamma(R)$. Moreover, as $N(p) \sim \text{Poi}(\rho\pi R^2)$, we have

$$c = \mathbb{P}(\text{point } p \text{ is } (\alpha, \beta)\text{-covered}) \geq \mathbb{P}(N \geq \Gamma(R)) = 1 - F_{\text{Poi}}(\Gamma(R)|\rho\pi R^2).$$

Therefore, the lower bound of c is given by (8). When $\rho\pi R^2$ is large enough, the normal distribution $\mathcal{N}(\rho\pi R^2, \rho\pi R^2)$ excellently approximates the Poisson distribution $\text{Poi}(\rho\pi R^2)$. Therefore, Eq. (8) can be approximated by (10). \square

Appendix 5: Proof of Lemma 6

Proof. Denote A_j as the event that the target is not detected in the j th unit detection. Thus, the probability of A_j is $\mathbb{P}(A_j) = 1 - P_{Dj}$. Suppose the target is detected in the J th unit detection. Although the intrusion detection is a series of infinite Bernoulli trials, J does not follow the geometric distribution because the success probability of each Bernoulli trial (*i.e.*, P_{Dj}) is a random variable rather than a constant. The mean of J is given by

$$\mathbb{E}[J] = 1 \cdot \mathbb{P}(\bar{A}_1) + \sum_{j=2}^{\infty} j \cdot \mathbb{P}\left(\bigcap_{k=1}^{j-1} A_k \cap \bar{A}_j\right) \quad (23)$$

$$\begin{aligned} &= 1 - \mathbb{P}(A_1) + \sum_{j=2}^{\infty} j \cdot \left(\mathbb{P}\left(\bigcap_{k=1}^{j-1} A_k\right) - \mathbb{P}\left(\bigcap_{k=1}^j A_k\right) \right) \\ &= 1 + \sum_{j=1}^{\infty} \mathbb{P}\left(\bigcap_{k=1}^j A_k\right) \end{aligned} \quad (24)$$

$$= 1 + \sum_{j=1}^{\infty} \prod_{k=1}^j \mathbb{P}(A_k) \quad (25)$$

$$= 1 + \sum_{j=1}^{\infty} \prod_{k=1}^j (1 - P_{Dk}). \quad (26)$$

Note that the $\bigcap_{k=1}^{j-1} A_k \cap \bar{A}_j$ in (23) represents the event that the target is not detected from the first to the $(j-1)$ th unit detection but detected in the j th unit detection. As the measurements in different sampling intervals are mutually independent, $\{A_j | j \geq 1\}$ are mutually independent. Hence, Eq. (25) follows. We now explain

the physical meaning of $\mathbb{E}[J]$. For a given randomly deployed network, if the target always appears at a fixed location and travels a fixed trajectory, according to (11), $\{P_{Dj}|j \geq 1\}$ are fixed values as $\{N_j|j \geq 1\}$ are fixed. As each unit detection is probabilistic, the $\mathbb{E}[J]$ is the average delay of detecting the target with fixed trajectory. For the target that appears at random location and travels arbitrary trajectory, $\{P_{Dj}|j \geq 1\}$ are random variables as $\{N_j|j \geq 1\}$ are random variables. Therefore, the average delay for detecting the target with arbitrary trajectory, *i.e.*, α -delay, is given by $\tau = \mathbb{E}[\mathbb{E}[J]]$, where $\mathbb{E}[\mathbb{E}[J]]$ is the average of $\mathbb{E}[J]$ taken over all possible target trajectories. If fusion ranges do not overlap, $\{N_j|j \geq 1\}$ are *i.i.d.* random variables. Hence, $\{P_{Dj}|j \geq 1\}$ are also *i.i.d.* random variables. Therefore,

$$\begin{aligned}\tau &= \mathbb{E}[\mathbb{E}[J]] = 1 + \sum_{j=1}^{\infty} \prod_{k=1}^j \mathbb{E}[1 - P_{Dk}] \\ &= 1 + \sum_{j=1}^{\infty} (1 - \mathbb{E}[P_D])^j = \frac{1}{\mathbb{E}[P_D]}.\end{aligned}$$

□

Appendix 6: Proof of Theorem 1

Proof. As ρ_f is large to provide a high level of spatial coverage under the fusion model, the lower bound of spatial coverage, c_L , is given by (10) according to Lemma 5. We define $h_1(\rho_f) = \frac{\Gamma(R)}{\sqrt{\pi}R} \cdot \frac{1}{\sqrt{\rho_f}}$, $h_2(\rho_f) = \sqrt{\pi}R \cdot \sqrt{\rho_f}$ and hence $c_L = Q(h_1(\rho_f) - h_2(\rho_f))$. When $\rho_f \rightarrow \infty$, $h_2(\rho_f)$ dominates $h_1(\rho_f)$ as $\lim_{\rho_f \rightarrow \infty} \frac{h_1(\rho_f)}{h_2(\rho_f)} = 0$. Hence, $c \geq c_L = Q(-h_2(\rho_f)) = Q(-\sqrt{\pi}R \cdot \sqrt{\rho_f})$ when $\rho_f \rightarrow \infty$. Define $x = Q^{-1}(c)$. We have $\rho_f \leq \frac{1}{\pi R^2} x^2$ when $c \rightarrow 1^-$.

Under the disc model, by replacing $c = Q(x) = 1 - \Phi(x)$ in (5) and solving ρ_d , we have $\rho_d = -\frac{1}{\pi r^2} \ln \Phi(x)$, where $\Phi(x)$ is the CDF of the standard normal distribution. Hence, we have

$$\lim_{c \rightarrow 1^-} \frac{\rho_f}{\rho_d} \leq \lim_{x \rightarrow -\infty} \frac{\frac{1}{\pi R^2} x^2}{-\frac{1}{\pi r^2} \ln \Phi(x)} = -\frac{r^2}{R^2} \lim_{x \rightarrow -\infty} \frac{x^2}{\ln \Phi(x)}.$$

As $\lim_{x \rightarrow -\infty} \frac{x^2}{\ln \Phi(x)} = -2$ [49], we have $\lim_{c \rightarrow 1^-} \frac{\rho_f}{\rho_d} \leq \frac{2r^2}{R^2}$. Therefore, the asymptotic upper bound of ρ_f is given by (13). □

Appendix 7: Proof of Theorem 2

Proof. We choose R by

$$\frac{\xi}{\pi} \cdot \frac{\Gamma(R)}{R^2} = \rho_f, \quad (27)$$

where ξ is a constant and $\xi > 1$. It is easy to verify that the chosen R is order-optimal for the lower bound of coverage (*i.e.*, c_L). Moreover, it is easy to verify that both the chosen R and $\Gamma(R)$ increase with ρ_f . By replacing ρ_f in (10) with (27), c_L is given by $c_L = Q\left(\left(\frac{1}{\sqrt{\xi}} - \sqrt{\xi}\right) \cdot \sqrt{\Gamma(R)}\right) = 1 - \Phi(\eta z)$, where $\eta = \frac{1}{\sqrt{\xi}} - \sqrt{\xi}$ is a constant and $z = \sqrt{\Gamma(R)}$. Hence we have $c \geq c_L = 1 - \Phi(\eta z)$. According to (5), the network density under the disc model satisfies $\rho_d = -\frac{1}{\pi r^2} \ln(1 - c) \geq -\frac{1}{\pi r^2} \ln \Phi(\eta z)$. Hence, the ratio ρ_f^b / ρ_d , where b is a positive constant, satisfies

$$\begin{aligned} \lim_{c \rightarrow 1^-} \frac{\rho_f^b}{\rho_d} &\leq \lim_{R \rightarrow \infty} \frac{\left(\frac{\xi}{\pi}\right)^b \cdot \frac{\Gamma^b(R)}{R^{2b}}}{-\frac{1}{\pi r^2} \ln \Phi(\eta z)} \\ &= -\frac{\xi^b r^2}{\pi^{b-1}} \cdot \lim_{z \rightarrow \infty} \frac{z^2}{\ln \Phi(\eta z)} \cdot \lim_{R \rightarrow \infty} \frac{\Gamma^{b-1}(R)}{R^{2b}} \\ &= \frac{2\xi^b r^2}{\pi^{b-1} \eta^2} \cdot \lim_{R \rightarrow \infty} \frac{\Gamma^{b-1}(R)}{R^{2b}}. \end{aligned}$$

Note that $\lim_{z \rightarrow \infty} \frac{z^2}{\ln \Phi(\eta z)} = -\frac{2}{\eta^2}$ [49] in the above derivation. As $w(x) = \Theta(x^{-k})$ and ϵ is constant, $\Gamma(R) = \Theta(1/w^2(R + \epsilon)) = \Theta((R + \epsilon)^{2k}) = \Theta(R^{2k})$ and hence $\Gamma^{b-1}(R) = \Theta(R^{2kb-2k})$. Therefore, $\lim_{R \rightarrow \infty} \frac{\Gamma^{b-1}(R)}{R^{2b}} = \lim_{R \rightarrow \infty} R^{2kb-2k-2b}$. If $b \leq \frac{k}{k-1}$, $\lim_{R \rightarrow \infty} \frac{\Gamma^{b-1}(R)}{R^{2b}}$ is a constant and hence $\lim_{c \rightarrow 1^-} \frac{\rho_f^b}{\rho_d}$ is upper-bounded by a constant. Hence, we have (14). We note that although the chosen R is not optimal for c , the upper bound given by (14) still holds if R is optimal for c . \square

Appendix 8: Proof of Lemma 7

Proof. We abuse the symbols a bit to use N instead of N_j and P_D instead of P_{D_j} as we are not interested in the index of unit detection. As $\rho \rightarrow \infty$, $N \rightarrow \infty$ almost surely. In (11), the second item $-\frac{\mu_s}{\sqrt{\sigma_s^2 + \sigma^2}} \cdot \sqrt{N}$ dominates when $\rho \rightarrow \infty$, since the first item $\frac{\sigma}{\sqrt{\sigma_s^2 + \sigma^2}} \cdot Q^{-1}(\alpha)$ is a constant. Therefore, it's safe to use $P_D = Q(\gamma \sqrt{N})$ to approximate (11), where $\gamma = -\frac{\mu_s}{\sqrt{\sigma_s^2 + \sigma^2}}$. From Lemma 2 and 6, if the same α -delay of τ is achieved under the two models, we have

$$\mathbb{E}[P_D] = 1 - e^{-\rho_d \pi r^2}. \quad (28)$$

We first prove the lower bound in (16). It is easy to verify that $P_D = Q(\gamma\sqrt{N})$ is a concave function. According to Jensen's inequality, we have $\mathbb{E}[P_D] \leq Q(\gamma\sqrt{\mathbb{E}[N]}) = Q(\gamma\sqrt{\rho_f\pi R^2})$. From (28), we have $1 - e^{-\rho_d\pi r^2} = \mathbb{E}[P_D] \leq Q(\gamma\sqrt{\rho_f\pi R^2})$. Accordingly, $\rho_d \leq -\frac{1}{\pi r^2} \ln \Phi(\gamma\sqrt{\pi R} \cdot \sqrt{\rho_f})$, where $\Phi(x) = 1 - Q(x)$. Hence, the density ratio satisfies

$$\lim_{\tau \rightarrow 1^+} \frac{\rho_f}{\rho_d} \geq -\pi r^2 \cdot \lim_{\rho_f \rightarrow \infty} \frac{\rho_f}{\ln \Phi(\gamma\sqrt{\pi R} \cdot \sqrt{\rho_f})} = \frac{2}{\gamma^2 R^2} \cdot r^2.$$

In the above derivation, we use the equality $\lim_{x \rightarrow \infty} \frac{x}{\ln \Phi(\eta\sqrt{x})} = -\frac{2}{\eta^2}$, which has been proved in [49].

We now prove the upper bound in (16). As $P_D > 0$, according to Markov's inequality, for any given number c , we have

$$\mathbb{E}[P_D] \geq c \cdot \mathbb{P}(P_D \geq c). \quad (29)$$

We define ξ and c as follows:

$$\xi = \frac{\gamma^2 + 2 - \sqrt{\gamma^4 + 4\gamma^2}}{2}, \quad c = Q(\gamma\sqrt{\xi\rho_f\pi R^2}). \quad (30)$$

It's easy to verify that $\xi \in (0, 1)$. Therefore,

$$\mathbb{P}(P_D \geq c) = \mathbb{P}\left(Q(\gamma\sqrt{N}) \geq Q(\gamma\sqrt{\xi\rho_f\pi R^2})\right) = \mathbb{P}(N \geq \xi\rho_f\pi R^2).$$

As $N \sim \text{Poi}(\rho_f\pi R^2)$ and the Poisson distribution approaches the normal distribution $\mathcal{N}(\rho_f\pi R^2, \rho_f\pi R^2)$ when $\rho_f \rightarrow \infty$, we have

$$\mathbb{P}(P_D \geq c) = Q\left(\frac{\xi\rho_f\pi R^2 - \rho_f\pi R^2}{\sqrt{\rho_f\pi R^2}}\right) = Q\left((\xi - 1)\sqrt{\rho_f\pi R^2}\right).$$

By replacing c and $\mathbb{P}(P_D \geq c)$ in (29), we have

$$\mathbb{E}[P_D] \geq Q\left(\gamma\sqrt{\xi\rho_f\pi R^2}\right) \cdot Q\left((\xi - 1)\sqrt{\rho_f\pi R^2}\right).$$

It is easy to verify that $\gamma\sqrt{\xi} = \xi - 1$. Thus the above inequality reduces to $\mathbb{E}[P_D] \geq Q^2(h\sqrt{\rho_f})$, where $h = \gamma\sqrt{\xi\pi R}$. From (28), we have $1 - e^{-\rho_d\pi r^2} = \mathbb{E}[P_D] \geq Q^2(h\sqrt{\rho_f})$. Accordingly, $\rho_d \geq -\frac{1}{\pi r^2} \cdot (\ln(1 + Q(h\sqrt{\rho_f})) + \ln \Phi(h\sqrt{\rho_f}))$. Hence, we have

$$\begin{aligned} \lim_{\tau \rightarrow 1^+} \frac{\rho_f}{\rho_d} &\leq -\pi r^2 \lim_{\rho_f \rightarrow \infty} \frac{\rho_f}{\ln(1 + Q(h\sqrt{\rho_f})) + \ln \Phi(h\sqrt{\rho_f})} \\ &= -\pi r^2 \lim_{\rho_f \rightarrow \infty} \frac{\rho_f}{\ln \Phi(h\sqrt{\rho_f})} = \frac{2}{\xi\gamma^2 R^2} \cdot r^2. \end{aligned} \quad (31)$$

Note that $h = \gamma\sqrt{\xi\pi}R < 0$ and $\ln(1 + Q(h\sqrt{\rho_f})) = \ln 2$ when $\rho_f \rightarrow \infty$. We also use the aforementioned equality $\lim_{x \rightarrow \infty} \frac{x}{\ln \Phi(\eta\sqrt{x})} = -\frac{2}{\eta^2}$ [49] to derive (31). \square

Appendix 9: Proof of Theorem 4

Proof. In Lemma 7, γ depends on the PSNR δ , *i.e.*,

$$\gamma = -\frac{\mu_s}{\sqrt{\sigma_s^2 + \sigma^2}} = -\frac{S_0\mu_0}{\sqrt{S_0^2\sigma_0^2 + \sigma^2}} = -\frac{\mu_0}{\sqrt{\sigma_0^2 + \frac{1}{\delta^2}}},$$

where μ_0 and σ_0^2 (both defined in the proof of Lemma 4) are constants. Moreover, ξ is a function of γ (given by (30)). Accordingly, γ and ξ are both constants when δ is fixed or approaches infinity. Hence, according to Lemma 7, the tight bound of the density ratio is $\lim_{\tau \rightarrow 1^+} \rho_f/\rho_d = \Theta(r^2)$. As $w^{-1}(x) = \Theta(x^{-1/k})$, according to (4), $r^2 = \Theta\left(\left(\frac{\delta}{Q^{-1}(\alpha)}\right)^{2/k}\right)$ for fixed β . Therefore, we have (17). \square

Appendix 10: Proof of Lemma 8

Proof. Let A_j denote the event that the target is not detected in the j th unit detection and C_j denote the corresponding target disc. Suppose the target is detected in the J th unit detection. Recall (24), we have $\mathbb{E}[J] = 1 + \sum_{j=1}^{\infty} \mathbb{P}\left(\bigcap_{k=1}^j A_k\right) = 1 + \sum_{j=1}^{\infty} \prod_{k=1}^j \mathbb{P}\left(A_k \mid \bigcap_{l=1}^{k-1} A_l\right)$. The above derivation follows the definition of conditional probability. Let C denote the common area between the k th target disc and the union of all the previous target discs, *i.e.*, $C = C_k \cap \left(\bigcup_{l=1}^{k-1} C_l\right)$. Therefore, $C \geq 0$ and

$$\begin{aligned} \mathbb{P}\left(A_k \mid \bigcap_{l=1}^{k-1} A_l\right) &= \mathbb{P}(\text{there is no sensor in } (C_k - C)) \\ &= e^{-\rho(\pi r^2 - C)} \geq e^{-\rho\pi r^2}. \end{aligned}$$

Hence, $\tau = \mathbb{E}[J] \geq 1 + \sum_{j=1}^{\infty} \left(e^{-\rho\pi r^2}\right)^j = \frac{1}{1 - e^{-\rho\pi r^2}}$. \square

Appendix 11: Proof of Lemma 9

Proof. We first introduce the generalized Hölder's inequality [15]. For random variables X_i , $i = 1, \dots, n$, we have $\mathbb{E}[\prod_{i=1}^n |X_i|] \leq \prod_{i=1}^n (\mathbb{E}[|X_i|^{p_i}])^{1/p_i}$ where $p_i > 1$ and $\sum_{i=1}^n p_i^{-1} = 1$. If X_i , $i = 1, \dots, n$, are identically distributed, by setting $p_i = n$, we have

$$\mathbb{E}\left[\prod_{i=1}^n |X_i|\right] \leq \mathbb{E}[|X|^n], \quad (32)$$

where X can be any X_i . In our problem, $\{N_j | j \geq 1\}$ are identically distributed random variables due to the Poisson process. As P_{D_j} is a function of N_j (given by (11)), $\{P_{D_j} | j \geq 1\}$ are also identically distributed random variables. Recall (26), by applying the inequality (32), the α -delay of fusion-based detection can be derived as

$$\begin{aligned} \tau &= \mathbb{E}[\mathbb{E}[J]] = 1 + \sum_{j=1}^{\infty} \mathbb{E}\left[\prod_{k=1}^j (1 - P_{Dk})\right] \\ &\leq 1 + \sum_{j=1}^{\infty} \mathbb{E}[(1 - P_D)^j] = \mathbb{E}\left[\frac{1}{P_D}\right]. \end{aligned}$$

□

Appendix 12: Proof of Theorem 5

Proof. According to Lemma 8 and Lemma 9, we have

$$1/(1 - e^{-\rho_d \pi r^2}) \leq \tau \leq \mathbb{E}[1/P_D]. \quad (33)$$

We first find an upper bound of $\mathbb{E}[1/P_D]$. As discussed in the proof of Lemma 7, it is safe to use $P_D = Q(\gamma\sqrt{N})$ to approximate (11), where $\gamma = -\frac{\mu_s}{\sqrt{\sigma_s^2 + \sigma^2}}$. As $N \sim \text{Poi}(\rho_f \pi R^2)$ and the Poisson distribution approaches to the normal distribution $\mathcal{N}(\rho_f \pi R^2, \rho_f \pi R^2)$ when $\rho_f \rightarrow \infty$, for any given constant $\xi \in (0, 1)$, we have $\mathbb{P}(N \geq \xi \rho_f \pi R^2) = Q\left(\frac{\xi \rho_f \pi R^2 - \rho_f \pi R^2}{\sqrt{\rho_f \pi R^2}}\right) = Q((\xi - 1)\sqrt{\rho_f \pi R^2})$. When $\rho_f \rightarrow \infty$, $\mathbb{P}(N \geq \xi \rho_f \pi R^2) \rightarrow 1$, i.e., $N \geq \xi \rho_f \pi R^2$ with high probability. Moreover, as $1/P_D = 1/Q(\gamma\sqrt{N})$ is a decreasing function of N , $\mathbb{E}[1/P_D] \leq 1/Q(\gamma\sqrt{\xi \rho_f \pi R^2})$ with high probability. Furthermore, according to (33), we have $1/(1 - e^{-\rho_d \pi r^2}) \leq 1/Q(\gamma\sqrt{\xi \rho_f \pi R^2})$ probability when $\rho_f \rightarrow \infty$. After manipulation, we have $\rho_d \geq -\frac{1}{\pi r^2} \ln(\Phi(\gamma\sqrt{\xi \pi R \sqrt{\rho_f}}))$, where $\Phi(x) = 1 - Q(x)$. Hence, we have

$$\lim_{\tau \rightarrow 1^+} \frac{\rho_f}{\rho_d} \leq -\pi r^2 \lim_{\rho_f \rightarrow \infty} \frac{\rho_f}{\ln(\Phi(\gamma\sqrt{\xi\pi R\sqrt{\rho_f}}))} = \frac{2}{\gamma^2 \xi R^2} \cdot r^2. \quad (34)$$

In the above derivation, we use the equality $\lim_{x \rightarrow \infty} \frac{x}{\ln \Phi(\vartheta\sqrt{x})} = -\frac{2}{\vartheta^2}$ that has been proved in [49]. Hence, the upper bound of the density ratio is $\lim_{\tau \rightarrow 1^+} \rho_f / \rho_d = \mathcal{O}(r^2)$. As $r^2 = \Theta\left(\left(\frac{\delta}{Q^{-1}(\alpha)}\right)^{2/k}\right)$, we have (18). \square

References

1. Ahmed, N., Kanhere, S.S., Jha, S.: Probabilistic coverage in wireless sensor networks. In: The 30th IEEE Conference on Local Computer Networks (LCN), pp. 672–681. Sydney, Australia (2005)
2. Ammari, H., Das, S.: Integrated coverage and connectivity in wireless sensor networks: A two-dimensional percolation problem. *IEEE Transactions on Computers* **57**(10), 1423–1434 (2008)
3. Bisnik, N., Abouzeid, A., Isler, V.: Stochastic event capture using mobile sensors subject to a quality metric. In: The 12th Annual International Conference on Mobile Computing and Networking (MobiCom), pp. 98–109. Los Angeles, CA, USA (2006)
4. Brass, P.: Bounds on coverage and target detection capabilities for models of networks of mobile sensors. *ACM Transactions on Sensor Networks* **3**(2), 9 (2007)
5. Cao, Q., Yan, T., Stankovic, J., Abdelzaher, T.: Analysis of target detection performance for wireless sensor networks. In: The 1st International Conference on Distributed Computing in Sensor Systems (DCOSS), pp. 276–292. Marina del Rey, CA, USA (2005)
6. Chair, Z., Varshney, P.K.: Optimal data fusion in multiple sensor detection systems. *IEEE Transactions on Aerospace and Electronic Systems* **22**(1), 98–101 (1986)
7. Chakrabarty, K., Iyengar, S.S., Qi, H., Cho, E.: Grid coverage for surveillance and target location in distributed sensor networks. *IEEE Transactions on Computers* **51**, 1448–1453 (2002)
8. Chen, W.P., Hou, J.C., Sha, L.: Dynamic clustering for acoustic target tracking in wireless sensor networks. *IEEE Transactions on Mobile Computing* **3**(3), 258–271 (2004)
9. Cheung, S.Y., Coleri, S., Dunder, B., Ganesh, S., Tan, C.W., Varaiya, P.: A sensor network for traffic monitoring (plenary talk). In: The 3rd International Symposium on Information Processing in Sensor Networks (IPSN). Berkeley, CA, USA (2004)
10. Clouqueur, T., Saluja, K.K., Ramanathan, P.: Fault tolerance in collaborative sensor networks for target detection. *IEEE Transactions on Computers* **53**(3), 320–333 (2004)
11. Davis, D., Davis, C.: *Sound System Engineering*. Focal Press, Taylor & Francis Group (1997)
12. Dousse, O., Tavouraris, C., Thiran, P.: Delay of intrusion detection in wireless sensor networks. In: The 7th ACM International Symposium on Mobile Ad Hoc Networking and Computing (MobiHoc), pp. 155–165. Florence, Italy (2006)
13. Duarte, M., Hu, Y.H.: Distance based decision fusion in a distributed wireless sensor network. In: The 2nd International Workshop on Information Processing in Sensor Networks (IPSN), pp. 392–404. Palo Alto, CA, USA (2003)
14. Duarte, M., Hu, Y.H.: Vehicle classification in distributed sensor networks. *Journal of Parallel and Distributed Computing* **64**(7), 826–838 (2004)
15. Finner, H.: A generalization of Hölder’s inequality and some probability inequalities. *The Annals of Probability* **20**(4), 1893–1901 (1992)
16. Flanagan, B.P., Parker, K.W.: Robust distributed detection using low power acoustic sensors. Tech. rep., The MITRE Corporation (2005). http://www.mitre.org/work/tech_papers/tech_papers_05/05_0329/

17. Gu, L., Jia, D., Vicaire, P., Yan, T., Luo, L., Tirumala, A., Cao, Q., He, T., Stankovic, J.A., Abdelzaher, T., Krogh, B.H.: Lightweight detection and classification for wireless sensor networks in realistic environments. In: The 3rd ACM Conference on Embedded Networked Sensor Systems (SenSys), pp. 205–217. San Diego, CA, USA (2005)
18. Gui, C., Mohapatra, P.: Power conservation and quality of surveillance in target tracking sensor networks. In: The 10th Annual International Conference on Mobile Computing and Networking (MobiCom), pp. 129–143. Philadelphia, PA, USA (2004)
19. Hata, M.: Empirical formula for propagation loss in land mobile radio services. *IEEE Transactions on Vehicular Technology* **29**(3), 317–325 (1980)
20. He, T., Krishnamurthy, S., Stankovic, J.A., Abdelzaher, T., Luo, L., Stoleru, R., Yan, T., Gu, L., Hui, J., Krogh, B.: Energy-efficient surveillance system using wireless sensor networks. In: The 2nd International Conference on Mobile Systems, Applications, and Services (MobiSys), pp. 270–283. Boston, MA, USA (2004)
21. Hefeeda, M., Ahmadi, H.: A probabilistic coverage protocol for wireless sensor networks. In: The 15th IEEE International Conference on Network Protocols (ICNP), pp. 41–50. Beijing, China (2007)
22. Kumar, S., Lai, T.H., Arora, A.: Barrier coverage with wireless sensors. In: The 11th Annual International Conference on Mobile Computing and Networking (MobiCom), pp. 284–298. Cologne, Germany (2005)
23. Kumar, S., Lai, T.H., Balogh, J.: On k -coverage in a mostly sleeping sensor network. In: The 10th Annual International Conference on Mobile Computing and Networking (MobiCom), pp. 144–158. Philadelphia, PA, USA (2004)
24. Lazos, L., Poovendran, R., Ritcey, J.A.: Probabilistic detection of mobile targets in heterogeneous sensor networks. In: The 6th International Symposium on Information Processing in Sensor Networks (IPSN), pp. 519–528. Cambridge, MA, USA (2007)
25. Li, D., Hu, Y.H.: Energy-based collaborative source localization using acoustic micro-sensor array. *EUROSIP Journal on Applied Signal Processing* **2003**(4), 321–337 (2003)
26. Li, D., Wong, K., Hu, Y.H., Sayeed, A.: Detection, classification and tracking of targets in distributed sensor networks. *IEEE Signal Processing Magazine* **19**(2), 17–29 (2002)
27. Li, X.Y., Wan, P.J., Frieder, O.: Coverage in Wireless Ad Hoc Sensor Networks. *IEEE Transactions on Computers* **52**(6), 753–763 (2003)
28. Liu, B., Dousse, O., Wang, J., Saipulla, A.: Strong barrier coverage of wireless sensor networks. In: The 9th ACM International Symposium on Mobile Ad Hoc Networking and Computing (MobiHoc), pp. 284–298. Hong Kong SAR, China (2008)
29. Liu, B., Towsley, D.: A study on the coverage of large-scale sensor networks. In: The 1st IEEE International Conference on Mobile Ad-hoc and Sensor Systems (MASS), pp. 475–483. Fort Lauderdale, FL, USA (2004)
30. Mainwaring, A., Culler, D., Polastre, J., Szewczyk, R., Anderson, J.: Wireless sensor networks for habitat monitoring. In: The 1st ACM International Workshop on Wireless Sensor Networks and Applications (WSNA), pp. 88–97. Atlanta, GA, USA (2002)
31. Meguerdichian, S., Koushanfar, F., Potkonjak, M., Srivastava, M.B.: Coverage problems in wireless ad-hoc sensor networks. In: The 20th IEEE International Conference on Computer Communications (INFOCOM), pp. 1380–1387. Anchorage, AK, USA (2001)
32. Meguerdichian, S., Koushanfar, F., Qu, G., Potkonjak, M.: Exposure in wireless ad-hoc sensor networks. In: The 7th Annual International Conference on Mobile Computing and Networking (MobiCom), pp. 139–150. Rome, Italy (2001)
33. NIST/SEMATECH: e-Handbook of Statistical Methods. The National Institute of Standards and Technology (NIST), Information Technology Laboratory, Statistical Engineering Division (2011). <http://www.itl.nist.gov/div898/handbook/>
34. Niu, R., Varshney, P.K.: Distributed detection and fusion in a large wireless sensor network of random size. *EURASIP Journal on Wireless Communications and Networking* **2005**(4), 462–472 (2005)
35. Nordio, A., Chiasserini, C., Viterbo, E.: Quality of field reconstruction in sensor networks. In: The 26th IEEE International Conference on Computer Communications (INFOCOM), pp. 2406–2410. Anchorage, AK, USA (2007)

36. Nordio, A., Chiasserini, C., Viterbo, E.: The impact of quasi-equally spaced sensor layouts on field reconstruction. In: *The 6th International Symposium on Information Processing in Sensor Networks (IPSN)*, pp. 274–282. Cambridge, MA, USA (2007)
37. Ren, S., Li, Q., Wang, H., Chen, X., Zhang, X.: Design and analysis of sensing scheduling algorithms under partial coverage for object detection in sensor networks. *IEEE Transactions on Parallel and Distributed Systems* **18**(3), 334–350 (2007)
38. Shakkottai, S., Srikant, R., Shroff, N.B.: Unreliable sensor grids: coverage, connectivity and diameter. In: *The 22nd IEEE International Conference on Computer Communications (INFOCOM)*, pp. 1073–1083. San Francisco, CA, USA (2003)
39. Sheng, X., Hu, Y.H.: Energy based acoustic source localization. In: *The 2nd International Workshop on Information Processing in Sensor Networks (IPSN)*, pp. 551–551. Palo Alto, CA, USA (2003)
40. Stroock, D.W., Varadhan, S.S.: *Multidimensional Diffusion Processes*, vol. 233. Springer (1979)
41. Tan, R., Xing, G., Liu, B., Wang, J., Jia, X.: Exploiting data fusion to improve the coverage of wireless sensor networks. *IEEE/ACM Transactions on Networking* **20**(2), 450–462 (2012)
42. Tan, R., Xing, G., Wang, J., Liu, B.: Performance analysis of real-time detection in fusion-based sensor networks. *IEEE Transactions on Parallel and Distributed Systems* **22**(9), 1564–1577 (2011)
43. Taylor, C., Rahimi, A., Bachrach, J., Shrobe, H., Grue, A.: Simultaneous localization, calibration, and tracking in an ad hoc sensor network. In: *The 5th International Symposium on Information Processing in Sensor Networks (IPSN)*, pp. 27–33. Nashville, TN, USA (2006)
44. Varshney, P.K.: *Distributed Detection and Data Fusion*. Springer, New York (1996)
45. Volgyesi, P., Balogh, G., Nadas, A., Nash, C.B., Ledeczi, A.: Shooter Localization and Weapon Classification with Soldier-Wearable Networked Sensors. In: *The 5th International Conference on Mobile Systems, Applications, and Services (MobiSys)*, pp. 113–126. San Juan, Puerto Rico (2007)
46. Wan, P.J., Yi, C.W.: Coverage by randomly deployed wireless sensor networks. *IEEE/ACM Transactions on Networking* **14**(Special issue on networking and information theory), 2658–2669 (2006)
47. Wang, W., Srinivasan, V., Chua, K.C.: Trade-offs between mobility and density for coverage in wireless sensor networks. In: *The 13th Annual International Conference on Mobile Computing and Networking (MobiCom)*, pp. 39–50. Montreal, QC, Canada (2007)
48. Wang, W., Srinivasan, V., Chua, K.C., Wang, B.: Energy-efficient coverage for target detection in wireless sensor networks. In: *The 6th International Symposium on Information Processing in Sensor Networks (IPSN)*, pp. 313–322. Cambridge, MA, USA (2007)
49. Xing, G., Tan, R., Liu, B., Wang, J., Jia, X., Yi, C.: Data fusion improves the coverage of wireless sensor networks. In: *The 15th annual international conference on Mobile computing and networking (MobiCom)*, pp. 157–168. ACM, Beijing, China (2009)
50. Xing, G., Wang, X., Zhang, Y., Lu, C., Pless, R., Gill, C.: Integrated coverage and connectivity configuration for energy conservation in sensor networks. *ACM Transactions on Sensor Networks* **1**(1), 36–72 (2005)
51. Yan, T., He, T., Stankovic, J.A.: Differentiated surveillance for sensor networks. In: *The 1st ACM Conference on Embedded Networked Sensor Systems (SenSys)*, pp. 51–62. Los Angeles, CA, USA (2003)
52. Zhang, H., Hou, J.: On deriving the upper bound of α -lifetime for large sensor networks. In: *The 5th ACM International Symposium on Mobile Ad Hoc Networking and Computing (MobiHoc)*, pp. 121–132. Tokyo, Japan (2004)
53. Zou, Y., Chakrabarty, K.: Sensor deployment and target localization based on virtual forces. In: *The 22nd IEEE International Conference on Computer Communications (INFOCOM)*, vol. 2, pp. 1293–1303 (2003)